Universität Zürich[UZH]

Geographisches Institut

Overland flow in the Studibach (Alptal, Switzerland): Testing an electrical resistance sensor approach

GEO 511 Master's Thesis

Author: Damian Pfenninger, 20-666-194

Supervised by: Dr. Ilja van Meerveld

Faculty representative: Prof. Dr. Jan Seibert

16.01.2026

University of Zurich

Institute of Geography

Hydrology and Climate

MSc thesis GEO 511

Overland flow in the Studibach (Alptal, Switzerland):

Testing an electrical resistance sensor approach

Created by:

Damian Pfenninger

Triemlistrasse 124, 8047 Zurich

Student number: 20-666-194

damian.pfenninger@uzh.ch

Supervisor	Ilja van Meerveld
Faculty representative	Jan Seiber
Delivery on:	16.01.2026

Abstract

Overland flow (OF) is a key runoff generation mechanism in pre–Alpine headwater catchments, yet its spatial and temporal variability is difficult to quantify using plot based measurements alone. This study evaluates the use of low cost electrical resistance (ER) sensors for detecting OF in the Studibach catchment (Alptal, Switzerland) and examines patterns of OF occurrence in relation to precipitation characteristics, antecedent wetness conditions, and site properties. ER sensors were installed at 14 established runoff plot sites across three subcatchments, and 16 precipitation events exceeding 5 mm were analyzed. ER sensors captured rapid precipitation responses, with abrupt resistance declines coinciding with OF initiation. Across all site–event combinations, the median difference between ER and plot based OF onset was 2 min (mean: 22 min), indicating near synchronous detection within measurement resolution. Despite data gaps caused by logger failures, more than 70 % of deployed sensors produced usable data. OF occurrence exhibited threshold like behavior, with approximate catchment wide thresholds of 43 mm for combined wetness (ASI + P) and 18 mm for event precipitation. Pooled Spearman rank correlations showed that OF detection was primarily controlled by precipitation intensity, with the strongest relationship for the 10 min maximum intensity (I_{10}; $\rho = 0.34$, $p < 0.001$), followed by mean event intensity (I_{mean}, $\rho = 0.28$, $p = 0.005$). In contrast, P and ASI +P showed only weak and statistically non−significant associations. Antecedent soil moisture exhibited a consistent negative relationship with OF detection ($\rho = -0.39$, $p < 0.001$), indicating that OF generation was favored under comparatively dry pre−event conditions. No consistent relationships were found between OF detection and static site characteristics such as soil properties, topography, or vegetation type, suggesting that event−scale OF occurrence is governed primarily by dynamic precipitation characteristics rather than persistent spatial controls. Overall, the results demonstrate that low cost ER sensors can reliably detect the timing and spatial occurrence of OF under field conditions. While individual sensors are sensitive to data loss and local microtopographic variability, aggregation at the site scale improves robustness. ER sensors therefore represent a practical complement to runoff plots for investigating event–scale OF dynamics and hillslope runoff connectivity in heterogeneous headwater catchments, provided methodological limitations are acknowledged.

Table of contents

1. Introduction

Overland flow (OF) is a key contributor to streamflow during precipitation and snowmelt events (Gauthier et al., 2025). As the movement of water across the land surface, OF represents a vital component of catchment hydrology because it can rapidly increase streamflow during intense precipitation. In addition, OF can transport substantial amounts of sediment, nutrients, and solutes from hillslopes to the stream network (Chaves et al., 2009; Jansson & Strömberg, 2004). Experimental studies in Switzerland have further shown that high intensity precipitation applied to vegetated hillslopes underlain by low permeability Gleysols can generate significant OF, highlighting its role as an important runoff pathway under comparable conditions (Badoux et al., 2006; Scherrer et al., 2007). However, the generation of OF is highly variable in both space and time, as not all parts of a watershed produce OF during each event (Dunne & Black, 1970; Gauthier et al., 2025; Tarboton, 2003). This spatial and temporal variability reflects the interaction between event–specific precipitation characteristics and heterogeneous soil and land–surface properties within the watershed (Dunne & Black, 1970; Tarboton, 2003). The occurrence and magnitude of OF are influenced by both meteorological conditions and site characteristics. In particular, high–intensity precipitation events may exceed the soil's infiltration capacity, which leads to surface water accumulation and, consequently, to OF in the form of infiltration–excess OF(Horton, 1945; Horton, 1933). Depending on antecedent moisture conditions, large precipitation events can lead to soil saturation and saturation OF, which control the available soil storage prior to an event (Dunne & Black, 1970; Zehe & Sivapalan, 2008). Therefore, antecedent soil moisture represents a key control on the occurrence of OF. Once the soil approaches a critical wetness threshold, additional precipitation can trigger a disproportionately large increase in runoff (Zehe & Sivapalan, 2008). Once the soil approaches a specific wetness threshold, even additional precipitation can trigger a disproportionately large increase in runoff (Zehe & Sivapalan, 2008). Topographic factors such as slope angle and shape influence moisture conditions and therefore runoff processes as well. For example, concentrated flowlines are prone to generate OF more often (Loos & Elsenbeer, 2011). Vegetation also strongly influences OF by intercepting precipitation, stabilizing soil through roots, and enhancing infiltration (Mishra et al., 2022). Plant litter and stems also contribute to higher surface roughness, which slows down OF and promotes temporary water retention (Abrahams et al., 1994; Monger et al., 2022).

Understanding the spatial and temporal variability of OF is essential for effective watershed management, as it helps explain rapid streamflow responses to precipitation and informs flood management strategies, soil conservation efforts, and water quality protection measures. Improved knowledge of the conditions under which OF occurs is also critical for hydrological modelling and land management.

Despite several decades of research on hillslope runoff processes across a range of climatic settings, including temperate (Dunne & Black, 1970; Weiler & Naef, 2003), semi–arid (Mounirou et al., 2012) and tropical environments (Zwartendijk et al., 2020), uncertainties remain regarding the dominant runoff generation mechanisms and their controlling factors at the hillslope scale. To address these uncertainties, this study investigates the occurrence and spatial variability of OF in a pre–alpine headwater catchment using electrical resistance (ER) sensors in combination with runoff plot observations. ER measurements are based on the decrease in soil ER with increasing moisture and have previously been applied to detect flowing water in intermittent streams (Jaeger & Olden, 2012) and to identify OF occurrence on hillslopes (Zimmermann et al., 2014).

1.1 Objectives

Gauthier et al. (2025) demonstrated, based on 14 runoff plots installed across the Studibach catchment, that the occurrence of OF varies strongly in both space and time and generally occurs only once a cumulative event precipitation total of approximately 18 mm is exceeded. This threshold was derived from event–scale precipitation sums and does not explicitly account for precipitation intensity or antecedent soil moisture conditions.

The main objective of this study is to evaluate the usefulness of ER sensors as a cost effective and non–invasive method for detecting the occurrence, timing, and spatial extent of OF. To achieve this, ER sensor measurements are compared with runoff plot observations to evaluate whether ER sensors can reliably detect the timing, frequency, and spatial extent of OF across the catchment.

1.2 Research questions

To assess the applicability of ER sensors for detecting OF, this study addresses the following research questions. In addition to comparing ER sensors and runoff plots, the analysis examines how OF occurrence relates to selected site– and event–specific controlling factors.

- How do ER sensors and runoff plots compare in their ability to detect OF?
- Do ER sensors installed at the same measurement site (i.e. within a local sensor cluster on the same hillslope and vegetation type) show similar OF detection behavior?
- How is OF occurrence related to event characteristics (antecedent moisture conditions and precipitation amount and intensity) and site characteristics (topographic setting, soil properties, and vegetation type)?

2. Literature review

The following chapter reviews the current state of knowledge on OF, focusing on its definition, controlling factors, and commonly applied methods for OF detection.

2.1 What is overland flow (OF)?

OF refers to the downslope movement of water on the soil surface before it enters the stream network (Tarboton, 2003). It represents the initial phase of surface runoff generation (Emmett, 1970). The occurrence of OF is governed by the interaction between precipitation input, infiltration capacity, and soil storage. Depending on which of these processes restrict infiltration, two main mechanisms can be distinguished. These include infiltration–excess (Hortonian) overland flow (HOF) and saturation–excess overland flow (SOF).

HOF occurs when the intensity of the precipitation exceeds the infiltration capacity of the soil (Horton, 1933). During a storm, the infiltration rate usually decreases as the soil becomes wetter and the hydraulic gradient declines, eventually reaching the saturated hydraulic conductivity (K_{sat}). Once precipitation exceeds this limiting rate, water begins to accumulate at the soil surface, after which it flows downslope. The infiltration capacity is largely determined by soil structure, texture, and pore connectivity, since these properties regulate how quickly water can be transmitted through the soil (Hendriks, 2010).

SOF occurs when the soil profile becomes fully saturated and can no longer store additional water. Under these conditions, incoming precipitation or lateral subsurface inflow leads to surface ponding and subsequent OF (Dunne & Black, 1970). Low K_{sat} limits vertical and lateral drainage, causing the soil profile to reach saturation more rapidly during precipitation events (Hendriks, 2010). Such conditions are common in pre–alpine catchments with Gleysols or Flysch derived soils and are also characteristic of parts of the Studibach catchment, where low permeability horizons constrain drainage(Badoux et al., 2006; Srinivasan et al., 2002). In the context of SOF, subsurface water may re–emerge at the land surface and flow downslope as return flow, thereby contributing directly to surface runoff generation (Tarboton, 2003). This exfiltration can occur when lateral inflow within the soil exceeds its drainage capacity, when the groundwater table rises to or above the surface (i.e. perched groundwater), or when active macropores or soil pipes connect to the surface and release stored subsurface water (Elsenbeer & Lack, 1996; Feyen et al., 1996; Wainwright et al., 2000). Exfiltration and subsequent OF may also be triggered where subsurface flow paths are interrupted or redirected by human made or natural features, such as roads, soil compaction, or landslides (Megahan, 1983; Ziegler et al., 2001). In many cases, therefore, SOF represents a combination of precipitation, soil water and return flow.

2.2 Factors influencing OF occurrence

The occurrence of OF is controlled by a combination of meteorological conditions and site–specific characteristics. The following section reviews the key factors that influence OF generation on the hillslope scale.

2.2.1 Soil moisture

Soil moisture refers to the amount of water stored within soil layers and is commonly expressed as soil water content. In this context, the water retained within soil pore spaces, together with the degree of hydrophobicity, represents a key control on soil flow paths (Gerke et al., 2015). Consequently, soil moisture strongly influences how catchments respond to precipitation, as even small precipitation inputs can cause clear changes in soil water content and runoff (Penna et al., 2011). Moreover, the relationship between soil moisture and runoff is typically nonlinear and often shows pronounced threshold behavior (Penna et al., 2011). Once soil moisture exceeds a critical threshold, additional precipitation can rapidly shift the system from infiltration dominated conditions to enhanced runoff generation, which reflects a threshold response that is also discussed conceptually by Zehe and Sivapalan (2008). Importantly, such threshold dynamics have been observed across a wide range of climatic and landscape settings, thereby highlighting soil moisture as a central control on runoff processes (Penna et al., 2011; Zehe & Sivapalan, 2008). As soil moisture conditions before a precipitation event largely determine how much of that precipitation can infiltrate, antecedent soil moisture is a key factor in OF generation (Zimmermann et al., 2014). Depending on the initial soil state, it can have two opposing effects. Under wet antecedent conditions, the soil already contains a large amount of water, meaning that only a small additional precipitation input is needed to reach saturation and trigger SOF (Dehotin et al., 2015). In contrast, dry antecedent conditions can reduce infiltration capacity through the formation of hydrophobic surface layers in the topsoil during extended dry periods (Ferreira et al., 2015). As a result, precipitation intensities can exceed the temporarily reduced infiltration rates and generate HOF, even under relatively modest precipitation inputs (Horton, 1933, 1945). Numerous studies have examined how variations in antecedent wetness influence the magnitude and frequency of OF (Dehotin et al., 2015; Elsenbeer & Lack, 1996; Ferreira et al., 2016; Zimmermann et al., 2014).

The effect of antecedent wetness on runoff is also reflected in the relationship between cumulative precipitation and total stormflow. During dry periods, small storms generally produce low stormflow volumes, which are often mainly limited to inputs from near saturated riparian zones. In contrast, under wet antecedent conditions, higher stormflow values are typically observed, indicating that hillslope contributions are active (Penna et al., 2011). Overall, antecedent wetness is the dominant control at the seasonal scale, whereas its influence on short term variations in runoff generation is comparatively limited (Zimmermann et al., 2014).

2.2.2 Land cover

Vegetation has a strong influence on OF by intercepting precipitation, binding soil through root networks, and facilitating infiltration (Mishra et al., 2022). Vegetation also contributes to surface roughness through leaves, stems and litter, which slows OF, increases flow resistance and promotes local water retention (Abrahams et al., 1994; Monger et al., 2022). Conversely forests with a thicker organic litter layer tend to exhibit stronger hydrophobic responses, which in turn increase the likelihood and magnitude of HOF (Badoux et al., 2006). Root systems modify soil structure and pore connectivity. The development of root derived macropores enhances vertical infiltration and subsurface flow, thereby reducing the occurrence of OF (Weiler & Naef, 1998).

Runoff generation is strongly shaped by different land cover types, as grasslands and wetlands generally produce OF events more frequently and in larger quantities than forests (Gauthier et al., 2025). In addition, surface runoff dynamics are also affected by the internal structure of forests. Woodlands with a closed canopy often exhibit sparse undergrowth and comparatively low surface roughness, which in turn promotes faster OF. By contrast, woodland structures that increase surface roughness, such as canopy gaps, accumulations of woody debris, or dense understory vegetation, tend to slow OF by creating more heterogeneous flow pathways. This influence is particularly evident in wood pastures dominated by bracken, where dense ground vegetation reduces flow velocities by 12–20 % compared to established broadleaf woodland and by 19–27 % compared to grass dominated wood pasture (Monger et al., 2022). Differences in infiltration capacity are particularly pronounced. Soils beneath established woodland exhibited K_{sat} values that were approximately eight times higher than those in bracken dominated wood pasture and up to 80 times higher than those in grass dominated wood pasture. Accordingly, these findings suggest that upland habitats can be managed to reduce flood risk by increasing soil water storage and by moderating OF through the enhanced surface roughness created by dense vegetation. As a result, the onset of runoff is delayed and delivery rates to streams are reduce (Monger et al., 2022).

The activity of livestock on a meadow can substantially alter the properties of the surface soil. For example, trampling by cattle can reduce soil porosity and macropore connectivity, leading to lower infiltration rates and more frequent OF (Kurz et al., 2006; Pietola et al., 2005). In heavily trampled zones such as drinking areas, infiltration rates can fall to just 10–15 % of those in undisturbed pastures (Pietola et al., 2005), which highlights how sensitive soil hydraulic behavior is to compaction. In areas where the soil is already shallow or compacted, reducing grazing pressure can improve permeability by enhancing both surface roughness and K_{sat}. However, in well aerated soils, surface roughness becomes the more significant factor controlling OF (Monger et al., 2022).

2.2.3 Precipitation and Climate Change

Triggered OF depends greatly on the precipitation event’s intensity, duration and return period (Haacke & Paton, 2023). Higher precipitation intensities markedly increase the depth and volume of OF, showing a clear link between precipitation characteristics and runoff production (Haacke & Paton, 2023). According to Gauthier et al. (2025), when precipitation exceeds 18 mm OF occurs frequently. Because such precipitation amounts occur regularly, conditions favorable for OF are common. However, spatial variability in precipitation across the catchment leads to marked differences in OF occurrence (Buda et al., 2009).

Further studies have shown that high intensity artificial precipitation applied to vegetated hillslopes underlain by low permeability Gleysols in Switzerland has demonstrated that OF can represent a significant runoff pathway (Badoux et al., 2006, Scherrer et al., 2007). In these catchments the experiments demonstrated that OF comprised between 39 and 94 % of the applied precipitation (Badoux et al., 2006). Based on Haacke & Paton (2023), precipitation events with comparable intensities were classified into different impact levels, thereby highlighting the risk of misjudging an event's effects when storm intensity is considered alone. This, in turn, illustrates the need for improved methods to characterize and classify precipitation. In a subsequent temporal analysis spanning all four impact classes at three locations in Germany, it was shown that the most severe events occurred mainly during summer and that the number of impactful storms has steadily increased over the past thirty years. These local trends align with broader patterns, indicating that heavy precipitation events have very likely become both more frequent and more intense across most land areas where reliable observations are available (IPCC, 2023). At the continental scale, North America, Europe, and Asia have all seen increases in heavy precipitation. In Central Europe specifically, there is medium confidence that extreme precipitation has increased in either frequency or intensity (IPCC, 2023).

2.2.4 Topography

The frequency of OF is influenced by a combination of terrain features, flow path geometry, and surface conditions. Three key factors have been identified as being particularly important: microtopography, slope, and flow path length (Loos & Elsenbeer, 2011). At the onset of precipitation, surface characteristics determine where OF begins. Areas of flow convergence, such as concentrated flowlines and broad wash zones, tend to generate OF more frequently than dispersed hillslope elements, such as rills or swales (Loos & Elsenbeer, 2011). Slope plays a dual role in OF generation. Increasing slope steepness generally enhances runoff occurrence because steeper gradients promote faster lateral water movement and more efficient flow concentration. This also increases total and peak discharge, as higher flow velocities reduce the time available for transmission losses (Loos & Elsenbeer, 2011; Reaney et al., 2014). However, beyond a certain threshold, additional steepening can reduce OF due to shorter residence times and limited surface water accumulation (Loos & Elsenbeer, 2011). At the subsurface level, steeper slopes increase the hydraulic gradient and therefore promote faster downslope drainage.

Consequently, water is removed more quickly, which reduces the likelihood of a perched water table developing and thus limits the conditions required for SOF. Moreover, soil properties such as porosity, depth, texture, and hydraulic conductivity often differ systematically between steep and gentle terrain, and these variations, in turn, shape the generation of both SOF and HOF (Casanova et al., 2000; Pachepsky et al., 2001; Wierda et al., 1989). Slope length also influences runoff generation. Numerical modelling shows that longer slopes result in lower runoff coefficients because runoff remains on the slope for longer, allowing more water to infiltrate the soil after precipitation ceases (Reaney et al., 2014). Similarly, experimental work by Wainwright & Parsons, (2002) demonstrated that increasing slope length reduces the runoff coefficient, as water travelling over longer flow paths experiences greater transmission losses before reaching the slope outlet.

Surface roughness also controls runoff by determining how much water can be stored temporarily in surface depressions (Hu et al., 2020). As precipitation continues, the surface can be scoured and smoothed, which promotes crust formation. Both processes reduce infiltration and slightly increase outflow. Once the depressions have reached their storage capacity, any excess water spills over, resulting in a rapid increase in surface outflow (Hu et al., 2020).

One common approach to quantify local wetness based on topography is the Topographic Wetness Index (TWI). It is defined as TWI = $\ln(a/\tan\beta)$, where a represents the upslope contributing area per unit contour length (m) and β denotes the local slope (°). Many topography based hydrological models assume that locations with identical TWI values show similar groundwater responses because the local slope serves as an approximation of the hydraulic gradient, while the upslope contributing area controls the amount of subsurface flow directed toward the point of interest (Beven & Kirkby, 1979). The TWI is therefore commonly used to identify locations prone to SOF (Guentner et al., 1999). Ultimately, water exiting saturated patches may reach stream channels by flowing overland or by falling directly onto already saturated zones, thereby extending the channel network. These interconnected flow paths form dynamic surface responses that vary with precipitation and terrain configuration (Dunne & Black, 1970).

2.2.5 Soil and bedrock characteristics

Soil and bedrock properties strongly influence OF because they determine how readily precipitation can infiltrate into the subsurface. In particular, shallow or compacted soils, for example those affected by livestock trampling, limit pore space and reduce macropore connectivity. As a result, infiltration is greatly reduced and the likelihood of OF increases (Kurz et al., 2006;

Pietola et al., 2005). Similarly, soils with low porosity or low K_{sat} show reduced infiltration, which leads to faster and more widespread of OF (Yen & Akan, 1983). Similarly, thin soil layers with limited water storage capacity generate OF more quickly, as they cannot absorb or retain much precipitation (Wilcox et al., 2007). Differences in hydraulic conductivity at different depths, driven by soil development and rooting patterns, can create shallow horizons with low K_{sat} (Zimmermann et al., 2013). When low permeability layers are located close to the surface, water can build up above them during precipitation. As a consequence, local saturation develops, which promotes the generation of SOF. This mechanism has been shown to produce rapid and intense runoff responses in catchments where shallow permeability contrasts occur (Zimmermann et al., 2014).

Irrigation experiments conducted in Switzerland provide clear evidence that soil type has a strong influence on OF behavior (Scherrer, 1996). In pre–alpine and alpine environments, poorly drained soils, such as Gleysols, consistently exhibit high runoff coefficients and limited subsurface flow. In contrast, better drained soils, such as Cambisols and Regosols, generally show much lower runoff coefficients, with a greater dominance of subsurface flow and deep percolation. Badoux et al. (2006) confirmed these contrasts, reporting substantially higher runoff generation on Gleysols than on Cambisols under both artificial irrigation and natural precipitation. Consequently, OF typically dominates on Gleysols, whereas on Cambisols, subsurface flow is predominant, with only temporary OF occurring under specific conditions, such as the presence of hydrophobic litter layers (Badoux et al., 2006).

Bedrock characteristics also play a key role because more permeable bedrock promotes vertical drainage, reducing surface runoff; whereas impermeable bedrock leads to rapid surface saturation and increased OF (Fang et al., 2024). Collectively, these findings highlight that OF generation is not simply a function of precipitation intensity, but is also strongly influenced by subsurface permeability, soil structure and terrain configuration.

2.3 Common methods to measure OF

To investigate OF in the field, a range of observational and experimental methods has been developed. The following section reviews the most commonly applied approaches for detecting and quantifying OF.

2.3.1 Electrical resistance (ER) sensors

ER is a physical property that describes how strongly a material opposes the flow of an electric current. The ER approach is commonly applied in soil moisture studies, as the ER of soil decreases with increasing moisture content because water conducts electricity more efficiently than air filled pores (de Jong et al., 2020). In hydrological applications, ER is used to detect the presence of water by measuring changes in resistance between two electrodes placed in or on the soil surface. ER sensors record variations in resistance between the electrodes (Bhamjee & Lindsay, 2011; Blasch et al., 2002);with values decreasing when water is present, then increasing again under dry conditions (Assendelft & van Meerveld, 2019). ER sensors have been installed in intermittent streams to detect the presence of water (Jaeger & Olden, 2012) and have also been deployed on hillslopes to identify OF (Zimmermann et al., 2014). Moreover, several studies have demonstrated their effectiveness for monitoring hydrological dynamics across a wide range of environments. For instance, these sensors have been applied to investigate stormflow generation (Srinivasan et al., 2002), to detect the onset of ephemeral streamflow in wetlands (Goulsbra et al., 2009), and to analyze longitudinal connectivity in rivers (Jaeger & Olden, 2012). Overall, ER sensors provide direct, reliable, and easily interpretable information on wetting and drying dynamics at high temporal resolution (Blasch et al., 2004; Constantz et al., 2001). While ER sensors have previously been used to detect the occurrence of OF at individual locations (Zimmermann et al., 2014) and variations in the timing of OF generation have been investigated (Moody & Martin, 2015), the spatial and temporal persistence of OF and its hillslope–scale connectivity patterns have not yet been systematically examined using ER sensors. Due to their simplicity, affordability and robustness, ER sensors are particularly well suited to the distributed monitoring of OF processes in complex terrain (Assendelft & van Meerveld, 2019). Moreover, the high spatial and temporal resolution of ER data makes it possible to apply network based analytical frameworks more effectively, thereby improving the characterization of flow connectivity and dynamics (Masselink et al., 2017).

2.3.2 Runoff plots

Runoff plots, as applied by Gauthier et al. (2025), are small, bounded field installations designed to measure overland and shallow subsurface flow under natural precipitation conditions**.** The plots used in that study follow established methodologies described by Maier et al., (2021) and Weiler et al., (1999). Each plot, typically measuring 1 m by 3 m, is bordered by plastic barriers in order to prevent lateral inflow or outflow, and it includes both an OF gutter at the surface and a trench at the downslope end. The gutter collects surface runoff, whereas the trench intercepts shallow subsurface flow or topsoil interflow. Subsequently, both flow components are routed through hoses to upwelling Bernoulli tubes (UBeTubes) (Stewart et al., 2015), where water levels are recorded at high temporal resolution using pressure and conductivity loggers. Consequently, this setup allows continuous monitoring of the timing, magnitude, and type of near surface flow in response to precipitation. Similar runoff plot approaches have been used to investigate the processes involved in runoff generation on both agricultural and forested hillslopes (Badoux et al., 2006; Buda et al., 2009; Gascuel-Odoux et al., 1996) and they have also been applied to evaluate the impact of snowmelt and frozen soil on flow dynamics in Alpine environments (Bayard et al., 2005). Consequently, runoff plots provide valuable, quantitative data on the spatial and temporal variability of runoff generation under different soil, vegetation and topographic conditions (Gauthier et al., 2025).

Nevertheless, the installation of natural runoff plots is time consuming due to extensive field construction and subsequent laboratory processing (Schallner et al., 2021). Their setup can disrupt soil and vegetation structure, and the systems require regular onsite maintenance as well as post–event sample analysis. Moreover, they can be relatively costly (Schallner et al., 2021). Despite these drawbacks, runoff plots allow for continuous, high resolution digital measurements of flow dynamics (Gauthier et al., 2025). At the same time, these limitations highlight the need for complementary approaches that can capture OF occurrence with lower disturbance and greater spatial coverage, motivating the use of methods such as ER sensors.

2.3.3 OF detectors

OF detectors, as installed and analyzed by Sauter (2017), are field instruments designed to record the occurrence and timing of surface runoff during precipitation. In the Studibach catchment, they were implemented as OF collectors (OFCs) in accordance with the methodology of Zimmermann et al. (2014). Each OFC consists of a short, perforated pipe, with a diameter of 50 mm and a length of approximately 0.5 m, which is connected to a T–junction and a storage chamber. The perforations in the pipe collect surface runoff and very shallow subsurface water, and this water then drains into a chamber where it can be sampled and analyzed. Moreover, similar collector–type systems have been used to investigate runoff generation and surface connectivity across a wide range of climatic and geological settings, including tropical rainforest and agricultural catchments (Godsey et al., 2004; Vigiak et al., 2006). The collectors function as on–off detectors, indicating the presence or absence of OF during an event. They also serve as samplers for chemical or isotopic analyses. However, the chambers must be emptied manually after each event, which makes the method time consuming and limits the temporal resolution of the data.

To overcome these limitations, some OF detectors are equipped with ER sensors that record the exact timing of flow initiation. These sensors measure the voltage drop between electrodes installed at the soil surface. When surface water bridges the electrodes, the ER decreases sharply to indicate the initiation of flow (Moody & Martin, 2015). This system enables the frequency and timing of OF during natural precipitation to be quantified, while remaining relatively low cost and simple to replicate (Zimmermann et al., 2014; Sauter, 2017).

3. Material & Methods

The following chapter outlines the study area and the methods applied to assess OF occurrence using ER sensors in combination with runoff plot observations

3.1 Study site

The study was conducted in the Studibach catchment (Figure 1), a pre–alpine headwater catchment located in the Alptal valley, approximately 40 km southeast of Zurich, Switzerland (coordinates: 47.038° N, 8.717° E). The catchment is characterized by heterogeneous soils, mixed vegetation cover, and a humid mountain climate, which are typical features of Swiss pre–alpine landscapes. The 20 hectare catchment ranges in elevation from 1270 to 1650 m above sea level. Moreover, it has an average slope of 18°, with values ranging from flat (0°) to very steep (69°), as derived from a high resolution 0.5 m digital elevation model (SwissAlti3D, Swisstopo). In addition, the area is characterized by a humid climate, with an average annual temperature of 6 °C, ranging from −1 °C in January to 14 °C in July (Schleppi et al., 1998). Annual precipitation averages around 2,300 mm, with approximately 30 % falling as snow (Stähli & Gustafsson, 2006). Although precipitation is distributed relatively evenly throughout the year, the most intense storms typically occur in summer, from June to September, when precipitation occurs on average every other day (Fischer et al., 2017; van Meerveld et al., 2019).

Vegetation cover in the catchment area consists of about 55 % open coniferous forest (Figure 1), predominantly Norway spruce (*Picea abies L.*) with a ground layer of blueberry species

(*Vaccinium* spp.*)* (Hagedorn et al., 2000). The remaining 45 % is covered by grasslands and wetlands, which are mostly found in flatter areas and depressions. The upper part of the catchment, accounting for around 10 % of the total area, is used as summer
pasture (Rinderer et al., 2016).

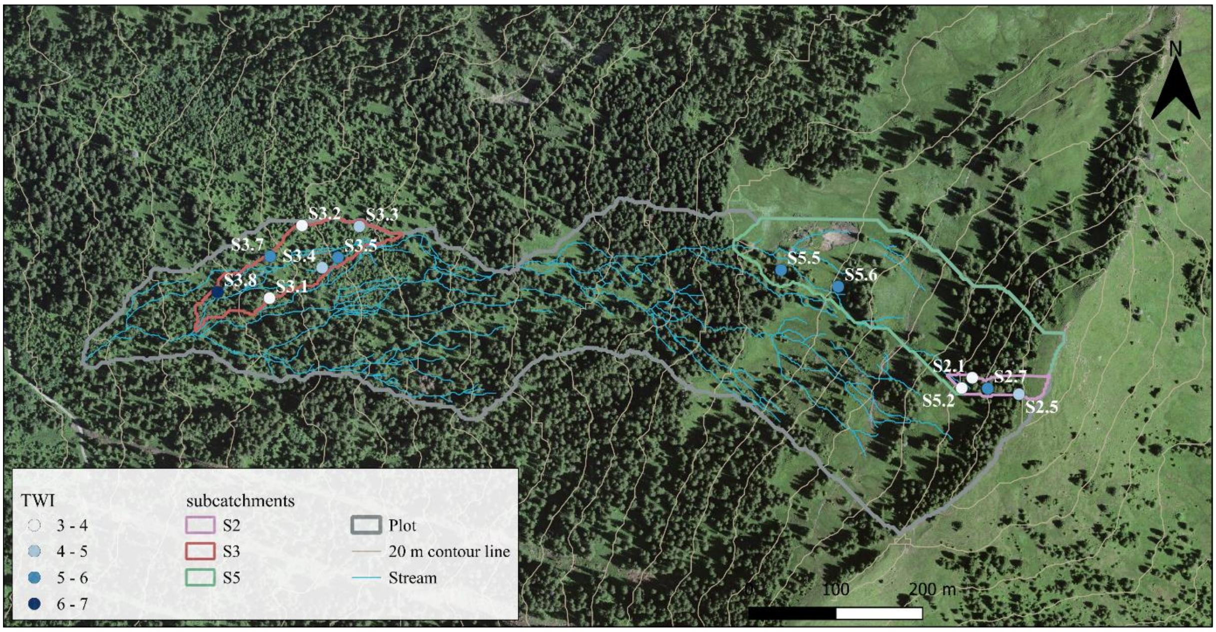

Figure 1 Overview map of the Studibach catchment displaying the locations of the monitored sites within the three subcatchments (S2, S3, and S5). The field surveyed stream network is shown in blue, and 20 m contour lines in gray. The background imagery represents vegetation derived from Swisstopo SwissImage (2025). Site colors correspond to the TWI, with darker blue tones indicating wetter areas.

The soils in the Studibach catchment are predominantly composed of silty clay and silt clay loam. The soils in this region are characterized by a clay–rich flysch bedrock with low permeability, comprising calcareous sandstone, argillite, and bentonite schist (Mohn et al., 2000). The depth of the soil varies depending on the landscape position, ranging from 0.5 to 1 m on the higher ridges and reaching up to 2.5 m in topographic depressions (Gauthier et al., 2025).

In areas of greater steepness, the soils are classified as umbric gleysols, which are characterized by the presence of an oxidized B_w horizon beneath a surface layer of mor humus. Conversely, the flatter, wetter parts of the catchment are characterized by mollic gleysols, where a reduced B_g horizon lies below a muck humus layer due to a consistently high water table (Hagedorn et al., 2001; Schleppi et al., 1998).

The combination of frequent precipitation and poorly permeable soils and bedrock results in generally shallow groundwater levels throughout the catchment (Rinderer et al., 2016). Such conditions favor the rapid development of saturated zones and promote SOF and return flow processes (Dunne & Black, 1970). This phenomenon is known to promote the development of a tightly connected stream network (Figure 1, van Meerveld et al., 2019 As a result, streamflow in such pre–alpine catchments often respond rapidly to precipitation, frequently within minutes. Although pre–event water is typically the dominant source of flow during storm events (Kiewiet et al., 2020) contributions from event water can exceed 50 % (Fischer et al., 2017; von Freyberg et al., 2018). Recent studies further indicate that a substantial fraction of event runoff can originate from water stored outside the actively flowing stream channels, particularly during the initial stages of runoff generation (Bujak–Ozga et al., 2024).

3.2 Microcontroller board and SD card data logger shield

The core of the monitoring system, as described by Assendelft & van Meerveld (2019), is based on the Arduino Pro Mini (5 V model), which is an open–source microcontroller board that uses the ATmega328 chip (Figure 2). Operating at 16 MHz, this board is equipped with 32 KB of flash memory, 2 KB of SRAM, and 1 KB of EEPROM. In addition, it provides 14 digital input and output (I/O) pins as well as six analogue input pins, all of which are compatible with internal pull–up resistors (20–50 kΩ). Moreover, two of the digital pins support external interruptions, while all six analogue pins are equipped with 10–bit analogue–to–digital converters (ADCs).

Figure 2 Microcontroller board and SD card data logger shield.

The Arduino Pro Mini was combined with an Adafruit SD card data logger shield, which integrates an SD card interface and a real time clock (RTC) powered by a 3 V lithium coin cell. Additionally, the shield provides a prototyping area that allows the Pro Mini to be soldered and wired directly onto it, since its smaller form factor and incompatible pin layout prevent conventional stacking. Furthermore, the SD card interface supports FAT16 and FAT32 file systems and allows long term data storage for up to several years, given the low memory requirements of each 60–bit data log entry. This setup was then configured as an interval logger using the Arduino IDE, with a logging frequency of one measurement every 5 min. The recorded data were timestamped via RTC and stored on a 2 GB SD card. Consequently, the configuration offered high efficiency, flexible programmability, and low cost, which made it particularly suitable for long term autonomous monitoring in remote field environments.

3.3 ER Sensor

The ER sensor used in this study is based on Assendelft & van Meerveld (2019) and consisted of two 1.8 mm diameter single core copper wires with polyvinyl chloride (PVC) insulation (Figure 3). The insulation was stripped off over the final 50 mm of each wire to serve as the electrode surface. This exposed length minimizes false detections and allows reliable measurement of the ER between the electrodes. The sensors were designed to detect the presence or absence of water by measuring the ER between the electrodes: low resistance indicates the presence of water, while high resistance indicates its absence.

Figure 3 ER sensor with its two electrodes including the V–shaped metal plates.

The sensor was connected to an Arduino–based data logger via a voltage divider circuit incorporating a 10 kΩ resistor. The resulting voltage drop was measured by the analogue pin and converted to resistance values using the following equation:

$$R = R_r / (\frac{1023}{ADCvalue - 1})$$

Where R represents the resistance between the ER sensor electrodes, R_r is the known resistor (10 kΩ), and ADCvalue is the output from the analogue–to–digital converter (ADC).

3.4 Selection of ER sensor locations

14 sites were selected and installed in two areas of the catchment to capture a range of slope gradients, vegetation types, and moisture conditions. The selection of plot locations was undertaken in accordance with the TWI (Beven & Kirkby, 1979) calculated from a 6 m resolution digital elevation model (DEM). In accordance with the approach adopted by Rinderer et al. (2014), who calculated TWI distributions for seven subcatchments, the present study divided each distribution into eight equal classes and identified the median TWI pixel in each class. The installation of groundwater monitoring wells was conducted in the designated median locations. For this study, three subcatchments (S2, S3 and S5) were selected for detailed analysis (Figure 1). Subcatchment S2 is located in the lower part of the Studibach catchment and includes a wide range of slope conditions. It is mainly covered by open coniferous forest, which is interspersed

with natural clearings as well as wetland areas (Figure 1). By contrast, subcatchment S3 is characterized by steeper terrain and dense forest cover, whereas S5 features gentler slopes where grasslands and wetlands are the dominant land cover types.

Given the strong correlation between groundwater dynamics and the TWI observed within this catchment (Rinderer et al., 2014; 2016), a TWI based stratification approach was used in order to capture spatial variation in hydrological processes more effectively than would be possible through random plot selection. Consequently, the selected runoff plots represent a broad range of topographic positions, moisture regimes, slopes, and vegetation types (Table 1).

To enable direct comparison between the runoff plots and the ER measurements, the site labels were renamed from CX.Y, as used in Gauthier et al. (2025), to SX.Y.Z. In this naming scheme, X denotes the subcatchment (S2, S3, or S5), Y refers to the TWI class ranging from 1 (driest) to 8 (wettest), and Z identifies the logger number within each site, for example ".1" for logger 1 and ".2" for logger 2. Furthermore, each logger was equipped with two sensors, OF1 and OF2, corresponding to sensor 1 and sensor 2, respectively.

3.5 Field measurements

This section describes the field measurements conducted in the Studibach catchment, including ER sensors, soil moisture measurements, and precipitation monitoring.

3.5.1 ER measurements

To measure OF, two metal plates were inserted into the soil in a V–shaped configuration, like illustrated in Figure 4, with the open side facing upslope and the tip directed downslope toward the valley. This setup was designed to collect and slow down surface runoff, allowing water to accumulate at the converging section of the plates. A small gap of a few centimeters was left between the plate tips to enable excess water to discharge through the opening. Two electrodes were placed within this gap 5 cm apart to measure the ER and determine the onset of OF as water passed through. The electrodes were connected to microcontroller boards. The ER measured between each pair of electrodes was used as the sensing signal, and each pair was therefore referred to as a sensor. Two sensors, named OF1 and OF2, were connected to a single microcontroller. In addition, a pair of electrodes were installed on each side of the microcontroller board behind the metal plate to detect subsurface flow. However, the subsurface flow data were not used in this study.

Figure 4 Field setup with metal plate (left) with the V–shaped configuration including the two electrodes placed in the 5 cm gap. Microcontroller board (right) with the OF1 and OF2 installed on each side.

At each site, either one or two microcontroller boards (loggers) were installed, resulting in two or four sensors per site and, overall, 21 loggers and 42 sensors across the Studibach catchment. In order to enable direct comparison with the runoff plots of Gauthier et al. (2025), the sensors were positioned in local depressions of the surface topography within 6 m of the plots. Furthermore, sensors connected to the same microcontroller were placed approximately 2 m apart. Nevertheless, the exact spacing varied slightly because soil and site conditions did not always allow the metal plates to be inserted at identical distances.

3.5.2 Soil moisture measurements

Soil moisture sensors (TEROS 12 and GS3, METER Group, USA) were installed at depths of 5, 20, and 30 cm below the surface along the edges of six runoff plots from Gauthier et al. (2025), namely C3.1, C3.4, C3.8, C5.2, C5.4, and C5.6. The sensors were connected to ZL6 and EM50 data loggers (METER Group, USA), which recorded soil moisture measurements at 5 min intervals.

3.5.3 Precipitation data

Precipitation data were collected using a tipping bucket rain gauge installed at the Erlenhöhe meteorological station, which is situated approximately 400 m from the Studibach catchment outlet at an elevation of 1215 m above sea level. The data, recorded at 10 min intervals, were provided by the Swiss Federal Institute for Forest, Snow and Landscape Research (WSL).

3.6 Site characteristics

Gauthier et al. (2025) conducted an assessment of several site–specific characteristics for each site (see Table 1). On the basis of this evaluation, the sites were classified into four main vegetation types, including open forest (F), natural clearings within the forest (C), grasslands (G), and wetlands (W). Forested sites are located in areas dominated by mature spruce trees, where the ground cover is largely composed of moss or blueberry shrubs, as observed at sites S2.1, S2.5, and S3.1. In addition, forested conditions may also occur in areas with younger tree growth, as illustrated by site S3.5. Natural clearings refer to small open spaces within a forest ecosystem that have developed naturally rather than through anthropogenic activities such as logging. These areas are typically covered by a combination of grasses, mosses, horsetail, alpine flowers, and blueberry bushes. Grasslands, by contrast, are defined as extensive open areas in which grasses and alpine flora dominate. Wetlands, finally, are characterized by the presence of sphagnum moss, horsetail, grasses, and alpine flowers.

The TWI values for each site were obtained from the analysis conducted by Rinderer et al. (2014). The measurement of site slope was conducted utilizing a handcrafted microtopographic profiler (Leatherman, 1987), whereby the elevation disparity between the upper and lower extremities of each site was calculated.

During the installation of the runoff trench, the depth of the A and B soil horizons was recorded as well. In addition, soil samples were collected from each site at a depth of 10–15 cm in order to assess organic matter content (OM), which was determined using the loss–on–ignition method.

Table 1 Key characteristics determined by Gauthier et al. (2025) of the sites include: TWI, soil depth at the base of the A and B horizons, slope, OM and vegetation type.

Site	TWI	Depth A horizon (cm)	Depth B horizon (cm)	OM (%)	Vegetation type	Slope (°)
S2.1	3.5	10	33	20	F	35
S2.5	4.5	10	39	13	F	26
S2.7	5.3	10	40		C	33
S5.2	4.1	5	31	3	G	27
S5.5	5.5	15	31	25	W	9
S5.6	5.9	15	> 40	23	W	14
S3.1	3.4	10	40	14	F	13
S3.2	4.1	15	30	20	C	19
S3.3	4.4	17	32	18	C	18
S3.4	4.8	20	40	11	C	15
S3.5	5.2	20	40	19	F	27
S3.7	6	18	35	48	C	21
S3.8	7	15	30	43	W	11

3.7 Data analysis

This section describes the methodological approaches used to identify OF events and to analyze the data in order to address the research questions of this study.

3.7.1 Precipitation event characteristics

The monitoring period was divided into 16 individual precipitation events, with each event being defined as a period during which more than 5 mm of precipitation occurred and which was separated from the preceding event by at least 12 hours without precipitation. Although Gauthier et al. (2025) analyzed 27 precipitation events, ER sensor data was available for only 16 events. For each event, total precipitation P (mm), the 10 min maximum intensity I_{10} (mm h^{-1}), mean precipitation intensity I_{mean} (mm h^{-1}), based on every 30 min precipitation period, and event duration D (min) were determined. Based on I_{mean}, events were classified into low

(< 2 mm h^{-1}), medium (2–4 mm h^{-1}), and high (> 4 mm h^{-1}) intensity categories. To describe antecedent wetness conditions, the Antecedent Soil Moisture Index ASI (mm) was calculated for the top 5 cm of soil using data from TEROS 12 and GS3 sensors installed at six runoff plots from Gauthier et al. (2025). For the ASI calculation, three sensors, namely C3.4, C3.8, and C5.2, were selected because they provided the most complete records and the most representative TWI values. Soil moisture readings were recorded at 5 min intervals, and the ASI was computed as the product of the average volumetric water content and the soil depth interval. Since ASI values at different depths were highly correlated ($r^2 > 0.99$), the top 5 cm were used to ensure consistency. Finally, the sum of the ASI and P was used as an indicator of overall wetness conditions ASI +P (mm) during each event (Detty & McGuire, 2010; Penna et al., 2011). An overview of all precipitation events and their associated characteristics is provided in Appendix A.

3.7.2 OF detection method

The procedure for detecting OF in the logger data comprised a structured sequence of five steps. The main filtering and detection criteria are summarized in the flow chart below (Figure 5) to provide an overview of the workflow. When a sensor for a given event passed all filtering criteria, it was considered a reliable detection of OF.

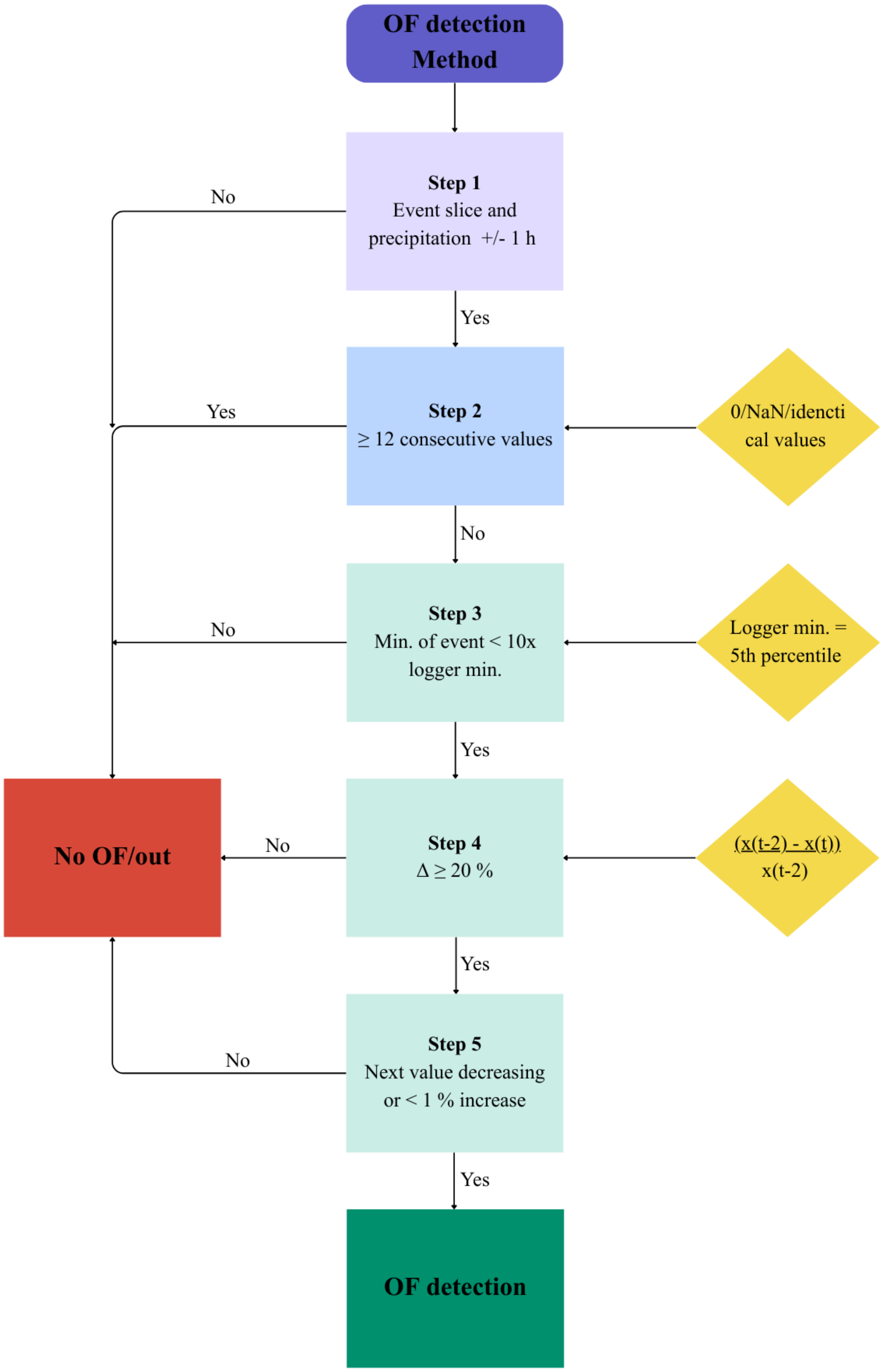

Figure 5 Flowchart of the OF detection and filtering procedure used to identify a distinct decline (OF onset). The method proceeded in five steps (explained below). Paths failing any step are labeled No OF/out; passing all steps yields OF detection.

Step 1: Event slicing

For each precipitation event, logger data were extracted following Gauthier et al. (2025) by starting one hour before the onset of recorded precipitation and ending one hour after precipitation had stopped. This temporal buffer was included to ensure that the full hydrological response was captured and, at the same time, to prevent subsequent reliability filters from excluding an event solely because of problematic data points occurring before or after the actual precipitation period.

Step 2: Reliability checks

The extracted event windows were initially checked for reliability. In cases where a window contained uninterrupted sequences of twelve zeros or more, corresponding to 1 hour of measurements, or where values were missing, it was discarded because such patterns typically indicate logger malfunction or data loss. Moreover, windows displaying twelve or more consecutive identical readings were interpreted as sensor flatlining rather than a genuine hydrological response and were therefore excluded. These reliability criteria are in line with established environmental monitoring practices, since long periods of unchanged measurements are widely regarded as clear signs of instrument malfunction (Campbell et al., 2013; Jones et al., 2017).

Step 3: Hydrological Plausibility Filter

The 5_{th} percentile of the raw time series was computed for each logger, with zeros and missing values being ignored in the computation. The rationale behind the selection of this low percentile is twofold: firstly, to eliminate the effect of isolated outliers, and secondly, to provide a more robust representation of the logger's background range. Within each event, the minimum value was then compared to this baseline. In instances where the minimum value of the event did not fall below ten times the 5_{th} percentile, the window was rejected for that specific logger. This criterion ensured that only events with values distinctly lower than the base distribution were retained, thereby increasing confidence that an actual OF response had occurred. The reason for this approach originated from the observation of exceedingly elevated readings in specific loggers and events, like in Figure 6, which made a simple comparison of raw values unfeasible. Figure 6 shows a sharp decline in resistance, which indicates a potential OF response. However, the recorded values remain far above the Q05 × 10 threshold. This suggests that despite the apparent drop, the data values are unrealistically high, rendering an actual OF measurement unlikely. In such cases, the window was rejected as the resistance values were outside the range expected for genuine OF conditions.

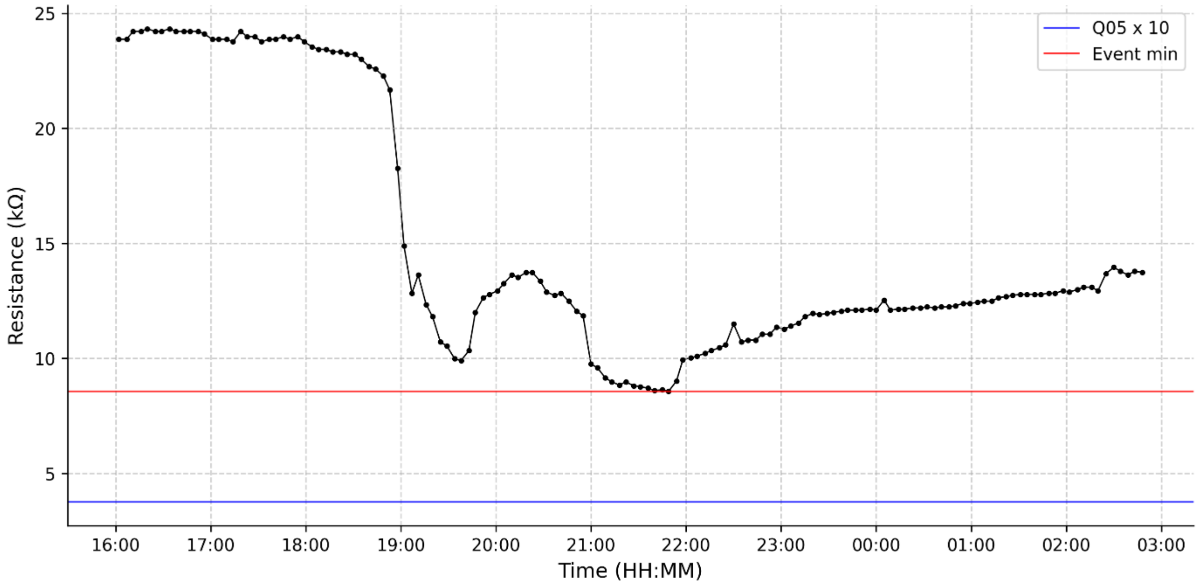

Figure 6 Event window ASI +P = 33 mm on 27 September. ER recorded by the sensor, with Q05 (blue line) representing the 5th percentile of the raw data for this sensor (multiplied by ten) and the event minimum (red line) indicating the lowest resistance measured within this event window.

Step 4: Threshold drop detection

At each time step within the remaining event windows, the current observation was compared to the measurement taken two steps earlier. A relative drop was defined as follows:

$$\frac{x_{t-2} - x_t}{x_{t-2}} > 0.20$$

If this threshold was exceeded, the time point was identified as a potential onset of OF. Using a two–step lag reduces sensitivity to small fluctuations and emphasizes distinct short term declines.

Step 5: Next–step validation

To reduce false detections, each candidate drop identified in Step 4 was validated by examining the subsequent observations. A candidate was accepted as the onset of OF when the value continued to decrease or, alternatively, when it increased by no more than one percent. In this way, the filtering approach was designed to eliminate cases such as the one shown in Figure 7, where isolated data spikes could otherwise lead to a false detection of an OF response. Figure 8 illustrates a further situation in which an OF signal appears to be present but does not exhibit a continuous decline, since the resistance value at 2521 Ω changes only marginally by less than one percent. If the following value displayed a more pronounced increase, the candidate was rejected. Consequently, this safeguard ensured that only sustained and hydrologically plausible declines were classified as genuine OF events. As a final step, all values ≥ 1’000’000 were removed from the dataset because they represent unrealistic measurements and therefore lack physical meaning. Nevertheless, the respective loggers were retained for further analysis, since these extreme peaks typically occurred at the beginning of the recordings, before the actual onset of OF.

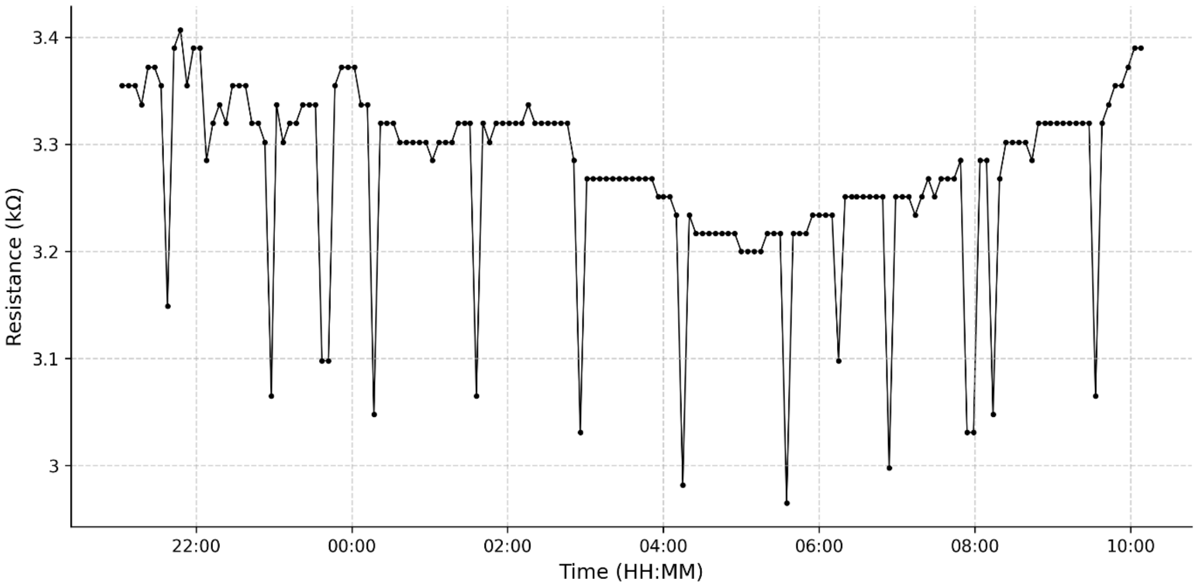

Figure 7 Event window ASI +P = 50 mm on 2 October. ER recorded by the sensor, with several singular abrupt decreases followed by immediate return to initial values.

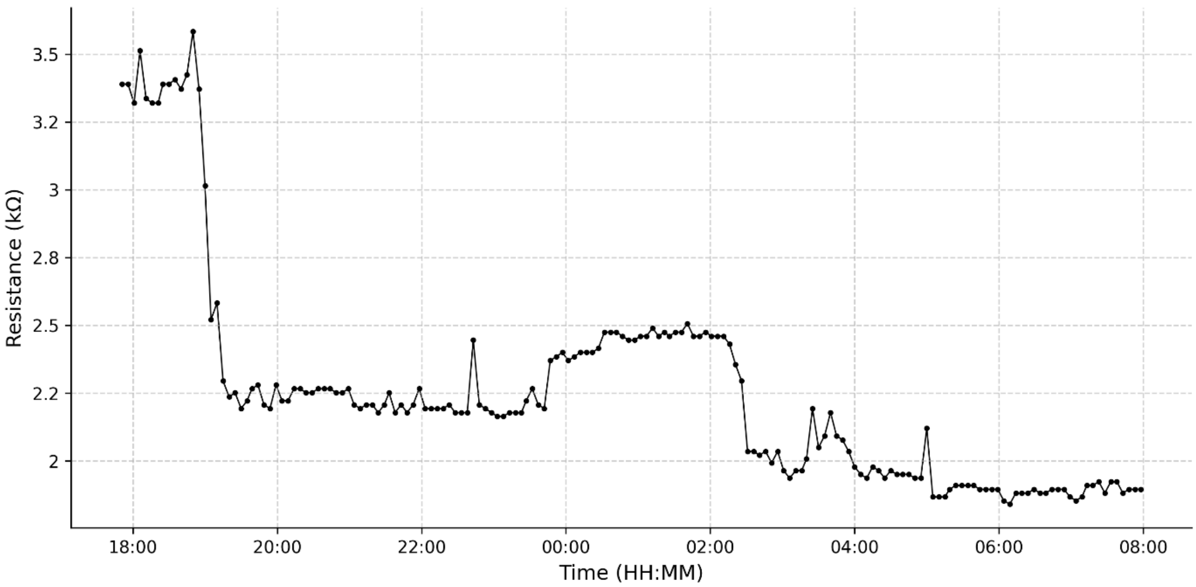

Figure 8 Event window ASI +P = 53 mm on 7 September. ER recorded by the sensor, where a clear OF signal is evident at 18:55; however, instead of a continuous decrease at 2521 Ω, a slight increase of less than 1 % is observed.

3.7.3 OF detection reliability & percentage

To assess the spatial consistency and data availability of OF measurements, the detection percentage of OF was calculated for each site and event (ASI + P). For this purpose, the time series recorded by each sensor for each event (ASI + P) were screened using the OF detection procedure described above. Sensors that failed any of these checks were classified as unreliable. By contrast, sensors that displayed valid signals were categorized as either "OF detection" or "no OF", depending on whether the detection threshold was reached. Sensors that contained only zeros or missing values over the entire duration of an event were instead classified as "no data". Accordingly, the resulting classification matrix summarizes the reliability and functionality of each sensor across all ASI + P events, thereby allowing malfunctioning loggers and temporal gaps within the dataset to be identified.

In addition, internal sensor consistency was examined at both logger and site levels. At the logger level, the two sensors, OF1 and OF2, were compared event–wise to determine whether they produced the same OF classification. However, this comparison was only conducted when both sensors returned valid data, meaning either "OF detection" or "no OF". Events in which only one sensor produced usable information were recorded but excluded from the comparison, which allowed cases of partial data loss to be distinguished from genuine disagreement in classification.

At the site level, all sensors installed at the same site were evaluated together. For each event, all valid OF classifications across the site were extracted, and agreement at the site level was determined using a majority–rule approach. Consequently, agreement was assigned when more than half of the available sensors indicated the same state. Events with only a single valid measurement were categorized as "no comparison", whereas events without valid data were ignored. Overall, this procedure ensured that sensor inconsistencies, data gaps, and spatial variability in OF detection were systematically quantified at both observation levels.

Because sites were equipped with either one or two loggers, each with two sensors, the number of available sensors per site ranged from two to four. As a result, the OF detection percentage is segmented in steps of 50 % for sites with two sensors and 25 % for sites with four sensors. This variability was retained explicitly and carried forward into subsequent analyses, while site–event combinations with missing or invalid sensor data were treated as no data and excluded from analyses requiring complete observations.

3.7.4 ER–runoff plot time differences

Time differences, including both mean and median values, were calculated to examine the temporal relationships between ER detection, runoff response, and precipitation. Three pairs were analyzed: (i) ER–runoff plot, (ii) runoff plot–precipitation, and (iii) ER–precipitation. For the ER–runoff plot pair, the ER timestamp was compared with both the runoff plot start time and the runoff plot peak time measured at the runoff plots. To characterize the earliest meaningful temporal linkage between ER detection and the runoff plot response, the smaller of the two time differences was retained, while the sign of the difference was preserved. This approach accounts for the fact that runoff at the plot outlet may begin to accumulate gradually before surface connectivity is established at the ER sensor location, such that the runoff plot start time can occur earlier than detectable ER wetting. In contrast, the runoff plot peak more reliably reflects fully developed and spatially connected flow conditions, which are more comparable to ER detection. Negative values indicate that runoff plot response occurred earlier, whereas positive values indicate that ER detection occurred earlier.

In addition, within–site similarity was assessed by extracting the smallest time gap between co–located sensors for each event and site. These gaps were then summarized in order to evaluate how similar the logger responses were.

3.7.5 ASI + P & P thresholds

Thresholds for OF were estimated using P and ASI + P by relating event-wise OF detection recorded as a binary response (YES/NO) for each logger and event to the corresponding predictor (either P or ASI + P). Records with missing predictor values were removed. Threshold estimation was conducted at the logger level to preserve the native event-wise detection information. Thresholds were reported only for loggers with a detectable breakpoint and at least seven valid events. Consequently, based on these criteria, no threshold was obtained for S2.1, S2.5, S3.4.2, S5.5.1, and S5.5.2. To determine global thresholds, all valid logger–event pairs were pooled across the study area, and a two-segment linear model was fitted to the detection–predictor relationship. The breakpoint associated with the smallest model error was identified as the global threshold. Only global thresholds are reported in the following analyses.

3.7.6 Statistical analyses

To examine the relationships between OF detection derived from ER sensors and potential controlling factors, pooled weighted Spearman rank correlation analyses were performed. Pooling observations across sites was necessary because the limited number of sensors per site (2–4) resulted in insufficient sample sizes for robust site-specific correlation analyses. Spearman's rank correlation coefficient (ρ) was used because it is non–parametric and, therefore, does not require the variables to be normally distributed or to follow linear relationships.

For all analyses, the response variable was defined as the percentage of OF detections per site and precipitation event, calculated as the proportion of sensors installed at a site that detected OF during a given event. Consequently, each observation represents a site–event combination, and each site contributes multiple observations corresponding to different precipitation events. Sites were equipped with one or two loggers, each containing two sensors, resulting in 2–4 sensors per site (mean: 3.23 sensors). Differences in the stability of percentage estimates were accounted for by weighting correlations according to the number of contributing sensors, while sites with fewer sensors were retained in the analysis.

In the first pooled analysis OF detection percentages were related to static site characteristics, including TWI, slope, vegetation type, and OM. Prior to the analysis, site names were standardized. Vegetation type was treated as a nominal categorical variable and therefore was not entered as an ordered rank. Instead, differences in OF detection percentages among vegetation classes (forest, clearing, grassland, wetland) were assessed using a non–parametric Kruskal–Wallis test. Correlations were then calculated across all available site–event combinations with valid data, meaning that observations were analyzed jointly rather than being evaluated separately for individual sites or events. The results were subsequently summarized by reporting Spearman's correlation coefficient (ρ), the associated p–value, and the number of site–event combinations included in each correlation.

In the second pooled analysis, the percentage of OF detections was correlated with precipitation event characteristics, including P, I_{10}, I_{mean}, ASI, and ASI + P. As in the analysis of site characteristics, all site–event combinations were evaluated jointly, thereby enabling the overall monotonic relationship between OF detection and event characteristics to be assessed across the full range of observed conditions. This pooled correlation analysis was conducted both for all precipitation events and for wet events only, which were defined as events with an ASI + P value greater than or equal to 42 mm. This threshold corresponds to the transition from moderate to high combined wetness conditions within the observed event distribution and was used to isolate events with elevated OF potential. For each subset, Spearman's correlation coefficient (ρ), the corresponding p–value, and the number of contributing site–event combinations were reported. All statistical analyses were carried out in Python 3.12 using the pandas, numpy, and scipy libraries.

4. Results

This chapter summarizes the results of the ER based analyses, beginning with a general overview of the data and observed response patterns. Subsequent sections examine relationships between ER observations and runoff plot data, followed by an assessment of spatial controls and precipitation related characteristics using statistical analyses.

4.1 Overview of the data

Several sites contained sensors with no data due to sensor malfunction or depleted batteries. Of the 14 installed ER sites, site S5.4 did not record any valid measurements throughout the study period and was therefore excluded from all analyses, resulting in a total of 13 sites. The number of active sensors per site ranged from two to four. The highest data coverage was achieved during events 10, 11, and 12, with ASI + P values of 53, 42, and 75 mm, respectively, when complete logger records were available from all but one site.

In the following, the terms sensor, logger, and site are used as follows. A sensor refers to a single ER measurement time series and corresponds to either OF1 or OF2. A logger consists of one microcontroller board connected to two sensors (OF1 and OF2). A site comprises one or two loggers and therefore includes two to four sensors in total. The naming convention reflects this hierarchy. For example, S3.2 denotes the site, S3.2.1 and S3.2.2 denote logger 1 and logger 2 at this site, respectively, and each logger contains the two sensors OF1 and OF2.

Across all sensors and events, 57 % of sensor–event records were classified as "no data", primarily due to sensor malfunction or dead batteries. These cases represent periods in which sensors were inactive and therefore excluded from further evaluation. Considering only sensor–event combinations with available data, 40 % detected OF, 32 % were classified as no OF, and 28 % were classified as unreliable. Combining OF detection and no OF (i.e. all functioning sensors) indicates that 72 % of available sensor records provided usable information. Despite the considerable number of inactive or failed sensors, these results demonstrate that the majority of sensor–event records with available data provided reliable measurements throughout the monitoring period. Overall, the reliability classification of the sensors varied between sites and events, reflecting differences in data quality and sensor performance which is illustrated in Figure 9.

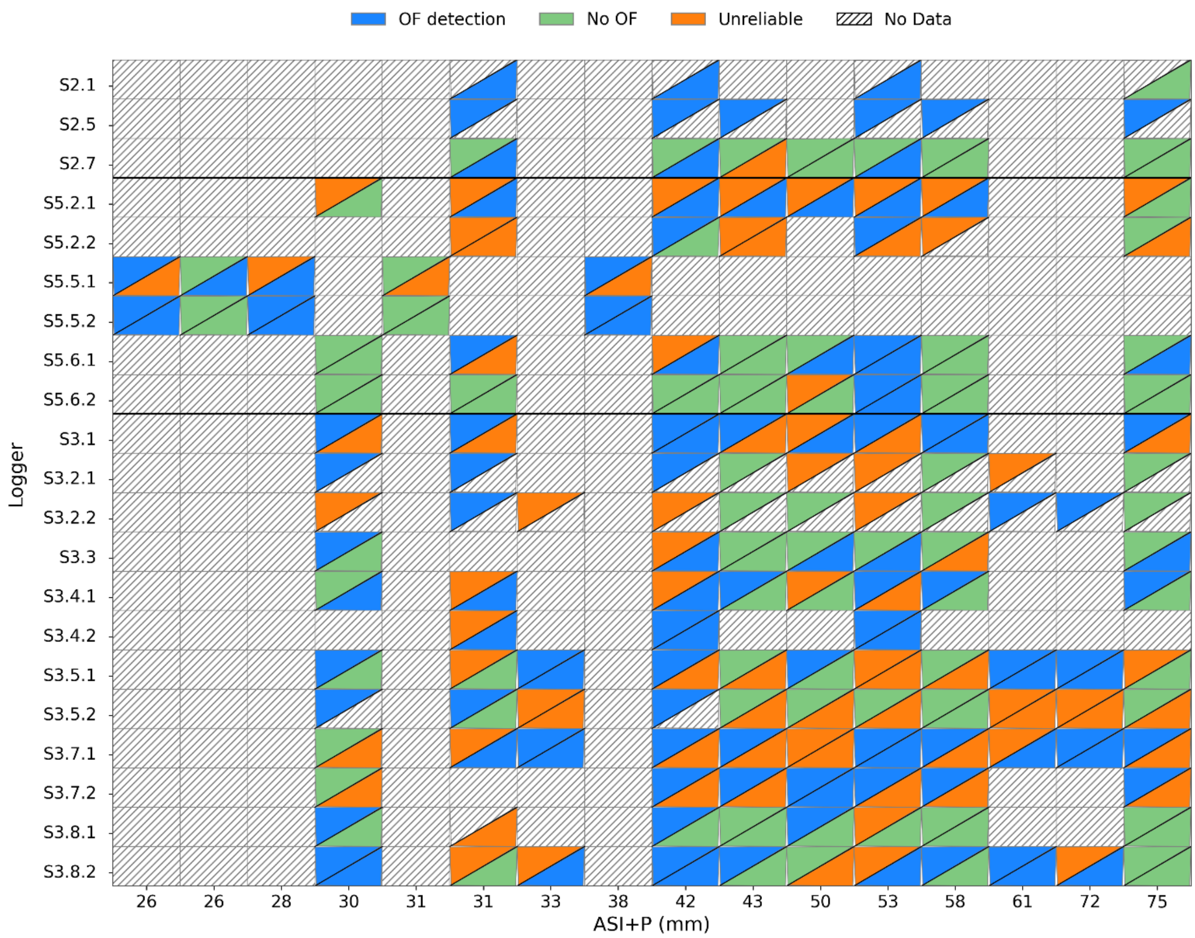

Figure 9 Heatmap of sensor reliability and OF detection by event (x–axis ordered by ASI + P) and logger (y–axis). Colored cells denote OF detection, no OF and unreliable data; hatched white cells indicate no data; diagonal line splits the information for OF1 (top) and OF2 (bottom).

Figure 9 further indicates that sensors and loggers installed at the same site generally showed consistent behavior, although the level of agreement clearly depends on the scale at which it is evaluated. At the logger scale, for example at S3.2.1, agreement was determined by directly comparing the two sensors connected to the same microcontroller, namely OF1 and OF2. Considering only events in which both sensors produced valid measurements, OF1 and OF2 agreed in 26 % of cases and disagreed in 15 % of cases. In the remaining 59 % of events, a comparison was not possible because only one of the two sensors returned to a usable value.

At the site scale, for example at S3.2, all sensors installed within the same site were evaluated jointly using a majority–rule approach. This aggregation combines the responses of all loggers and their associated sensors deployed within the site, such as OF1 and OF2 from S3.2.1 and S3.2.2, thereby allowing up to four sensors to contribute to a single site–level OF classification (see Figure 9). The site–level classification for each event was then assigned based on the most frequently observed OF class among the available sensors. Considering only events for which at least two valid sensor measurements were available, agreement was observed in 53 % of cases and disagreement in 12 % of cases. In the remaining 35 % of events, only a single valid measurement was available, which prevented a site–level comparison.

4.2 ER responses

Figures 10 and 11 illustrate the time series of ER at all monitored sites during event 11 on the 14th of September (ASI + P = 42 mm) and event 9 on the 2nd of September (ASI + P = 31 mm). The observed ER signals closely reflect the precipitation pattern, with increases in precipitation coinciding with decreases in ER. According to the OF detection method described in Section 3.7.2, such sustained resistance declines are classified as OF detections, indicating the onset of OF. For event 11 (Figure 10) OF was detected at all sites, although no data was available for S5.5. At three sites, both sensors, OF1 and OF2, recorded OF, whereas at the remaining sites either one sensor produced data or only one sensor detected a response. Importantly, all sensors that provided usable measurements during this event registered a response during the first and most intense precipitation peak at 16:40, when 6 mm of precipitation occurred within 30 min. Subsequently, the second precipitation peak at 19:00, with 3.5 mm within 30 min, also generated clear OF responses across all loggers. During the later and less intense precipitation peaks, however, OF was detected only at a subset of sites.

For event 9 (Figure 11) OF was detected at all sites except S5.5, where no data was available, and S3.8, where no OF occurred. This event was characterized by a single precipitation peak at 17:10, during which 7.1 mm of precipitation fell within 30 min. During this event, only one sensor (either OF1 or OF2) was active and able to detect a response at each site. As a result, no site displayed simultaneous detections by both sensors, which limits the assessment of logger–level consistency for this event.

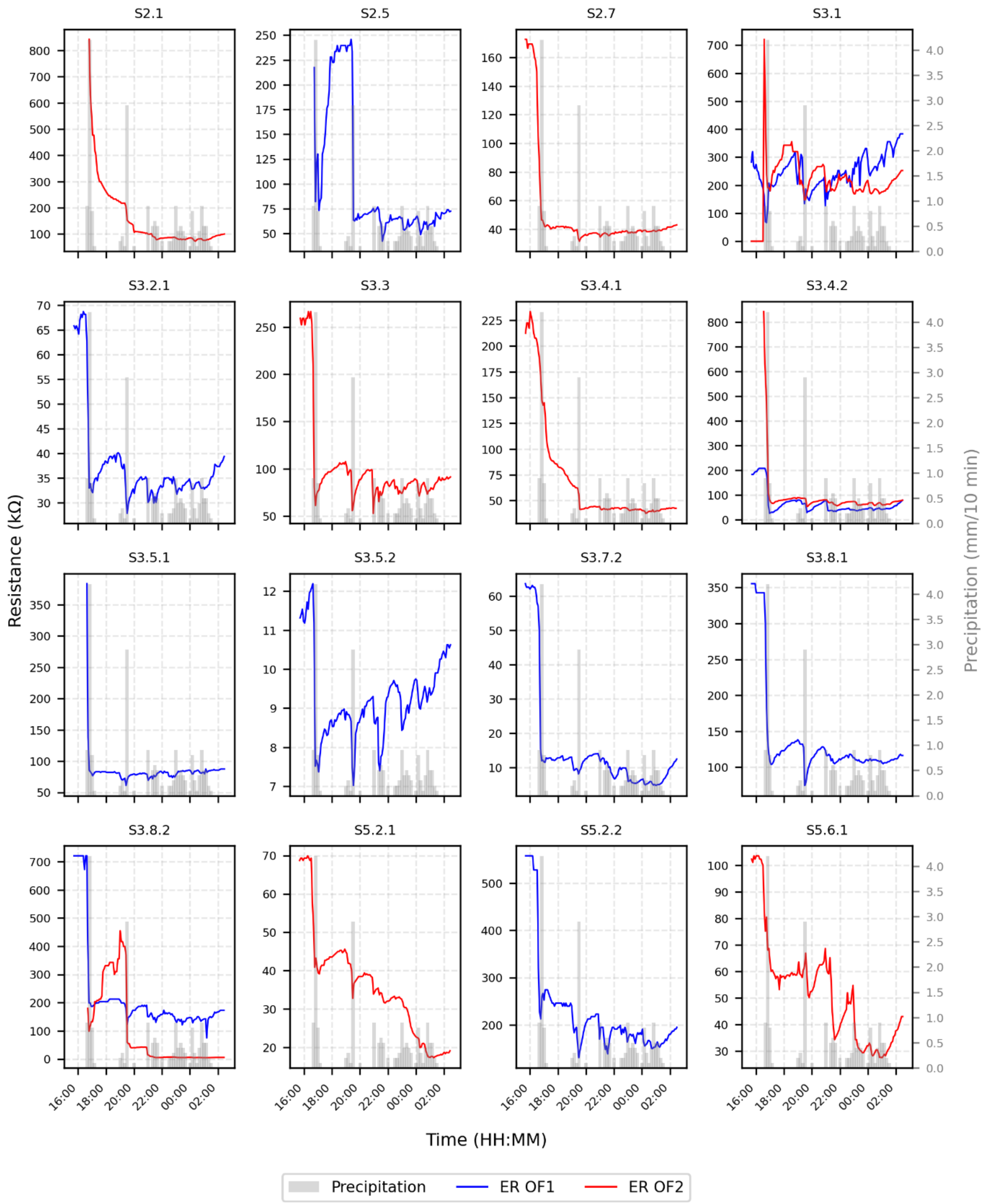

Figure 10 Time series of ER recorded by the OF1 (blue line) and OF2 (red line) sensors for each logger, together with the 10 min precipitation intensity (grey bars) for event 11 on the 14th of September (ASI + P = 42 mm). Note the different scale for the ER for each site.

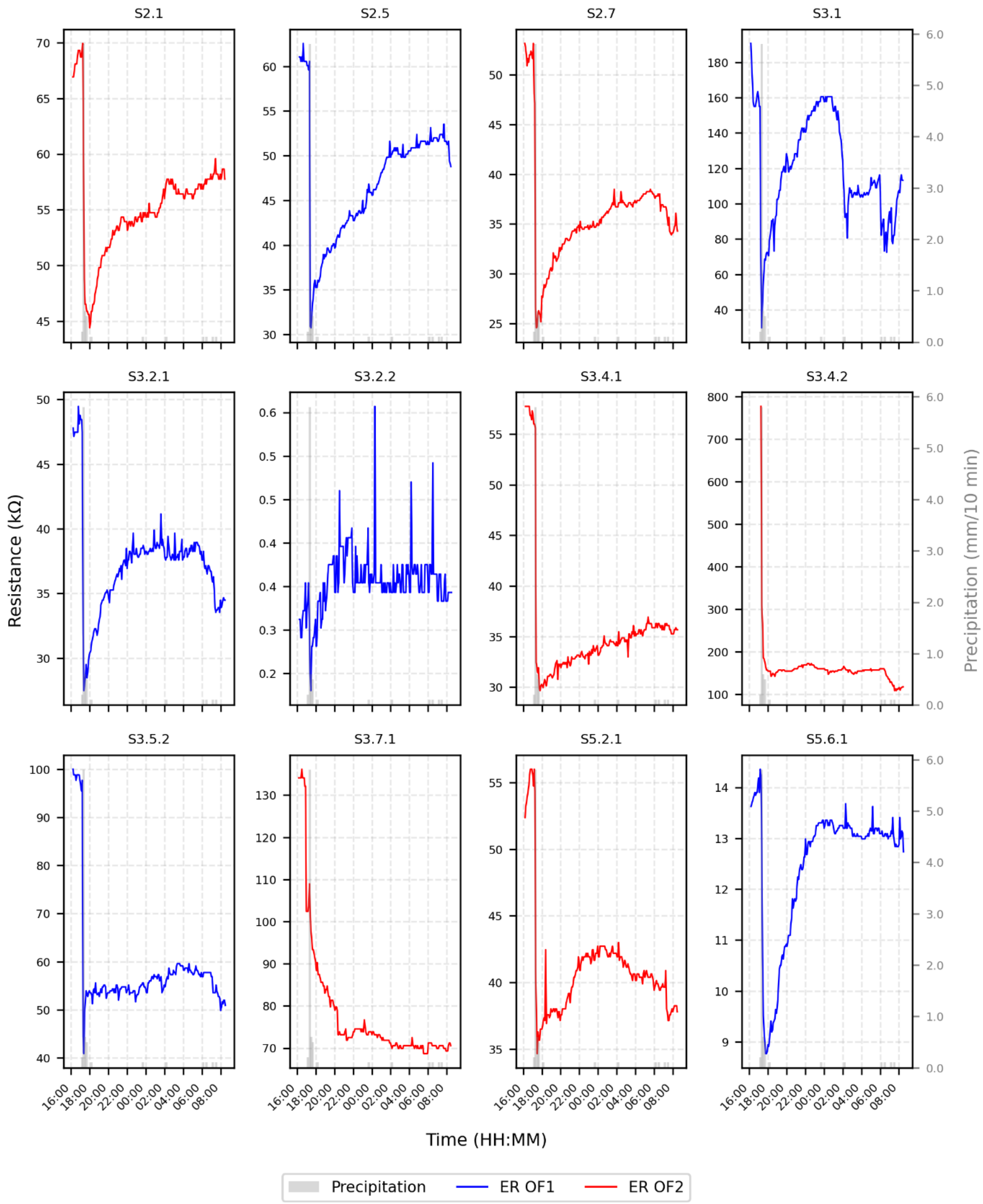

Figure 11 Time series of ER recorded by the OF1 (blue line) and OF2 (red line) sensor for each logger, together with 10 min precipitation intensity (grey bars) during event 9 on the 2nd of September (ASI + P = 31 mm). Note the different scales for the ER for each site.

4.3 ASI +OF detection

For event 11 OF was detected at 20 loggers, corresponding to an overall detection percentage of 53 % (Figure 12). Subsequent analyses are based on site–level detection percentages, obtained by aggregating sensor responses within each site for each event. When considering all events, the percentage of OF detections varied across both sites and events, with OF occurrence ranging from 0 % to 100 % of the sites (Figure 12). Overall, the median detection percentage was 25 %, while the average was 34 %.

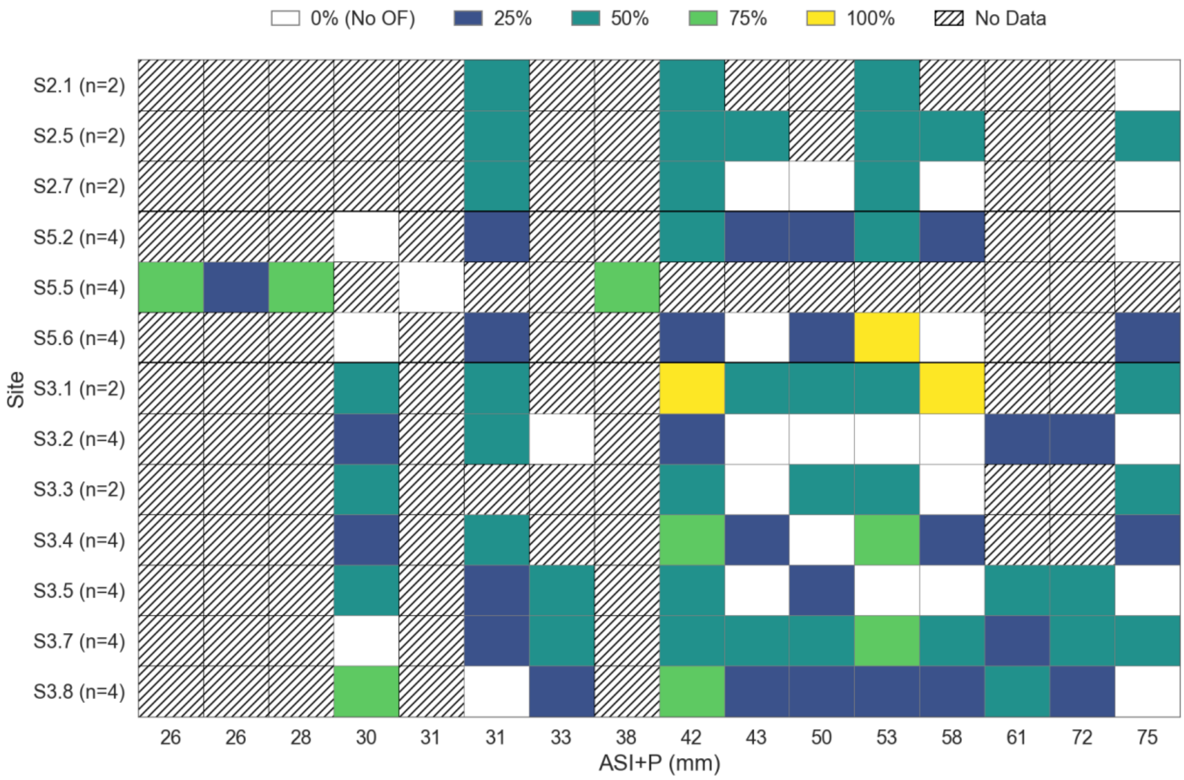

Figure 12: Heatmap the percentage of sites with working sensors for which OF was detected by event (x–axis ordered by ASI+P) and site (y–axis, where n refers to the number of sensors). White cells indicate 0 % OF detection (no OF detected at any of the sensors); dark blue indicates OF detected at all sensors; hatched cells indicate no data.

4.4 Comparison of ER–runoff plot data

This section compares ER–derived OF detections with runoff plot observations to evaluate the consistency between the two measurement approaches. The comparison focuses on the temporal correspondence of responses, their relationship to antecedent wetness and precipitation characteristics, and spatial patterns across sites. Together, these aspects provide insight into the degree of agreement between ER sensor detections and runoff plot responses under varying hydrometeorological and site conditions.

4.4.1 Timing

The rapid decline in ER occurred in close temporal alignment with the rapid increase in runoff from the plots at the onset of the precipitation event (Figure 13). After this initial drop, resistance increased gradually again during the recession phase while runoff decreased towards baseline levels.

For several site–event combinations ((e.g. Event 11) at S2.1, S5.2 and S3.2) there was a near–synchronous detection of OF at the runoff plot and by the ER sensors (see Figure 14). Across all data, the median difference between the timing of OF initiation based on the ER sensors and the measurements at the plot was 2 min (mean: 22 min), indicating that ER typically detected OF 2 min before it was measured at the runoff plot. The median time difference between the start of precipitation and the initiation of OF was 13 min for the plots and 12 min for the ER sensors, with corresponding means of 31 min and 51 min, respectively. In all comparisons, the means exceeded the medians, which is consistent with a small number of events having much longer time lags. However, for many site–event combinations, only one logger was detecting OF or was operational, preventing a more detailed within–site comparison.

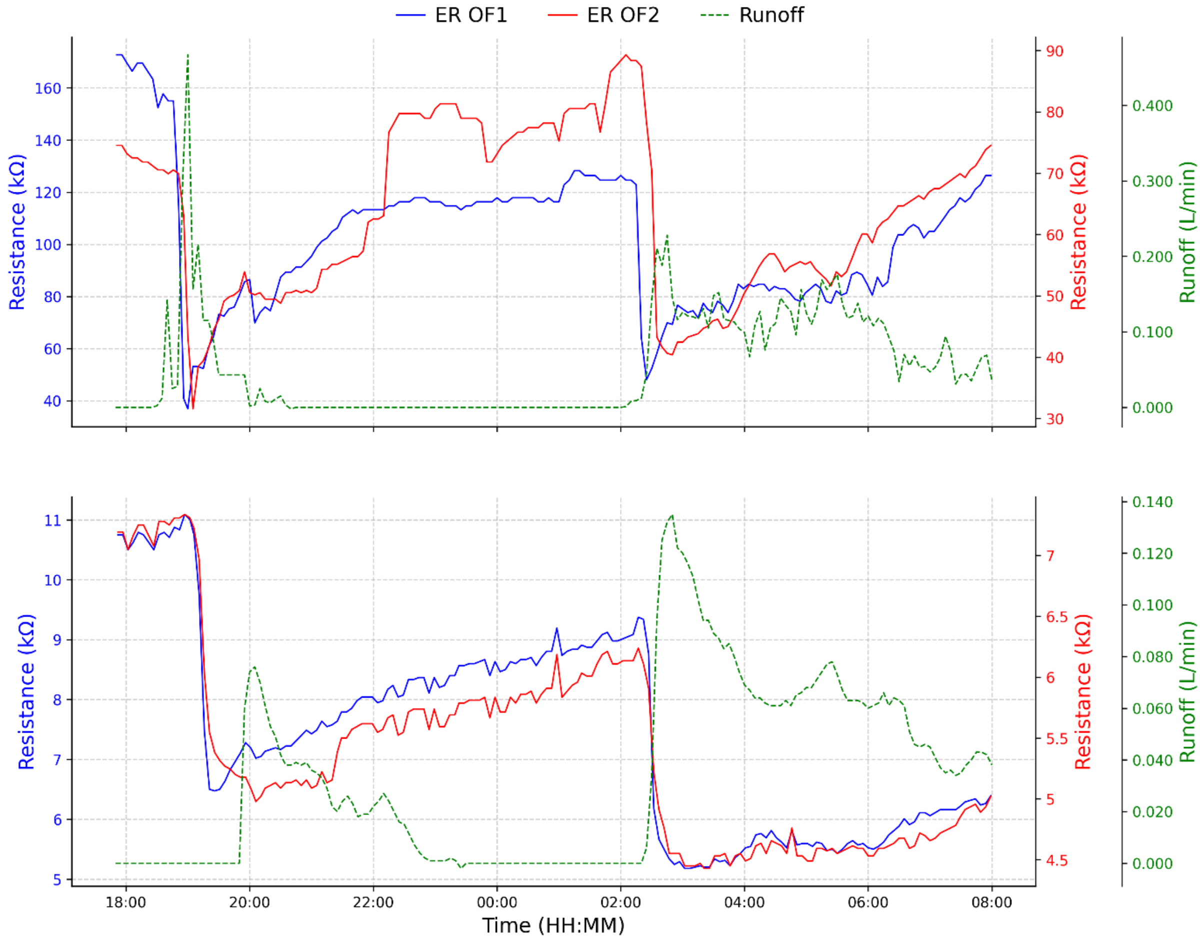

Figure 13 Time series of ER (OF1, blue; OF2, red) and runoff plot (green) during Event 10 (ASI + P = 53 mm) on 7 Sep 2022 at S3.4 (top) and S5.6 (bottom). At S3.4, ER OF1 exhibited notably higher resistance values than ER OF2. At S5.6, both ER curves followed a similar pattern with smaller amplitude changes than S3.4.

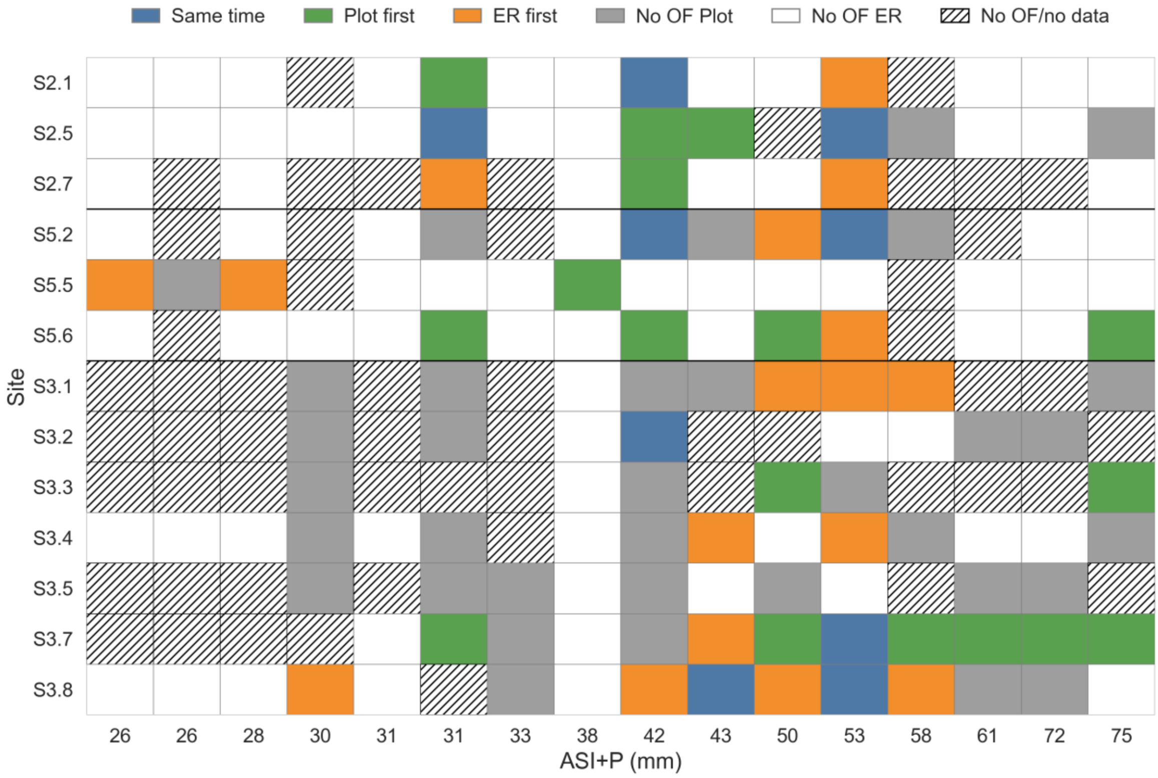

Figure 14 Heatmap illustrating the smallest absolute time difference in the onset of OF based on the measurements at the plot and ER sensors ordered for each site (y–axis) and event (x–axis, ordered by overall wetness (ASI + P)). Same response time is within 5 min (blue); Plot first (green); ER first (orange); No OF Plot (grey) meaning within the Plot no OF was detected; No OF ER (white) meaning within the ER no OF was detected; no OF/no data (hatched) meaning both methods didn't detect OF or missing data.

4.4.2 ASI +Wetness relationship

The threshold for OF occurrence across sites was approximately 43 mm for ASI + P and 18 mm for P (Figure 15). Site-specific thresholds varied, ranging from 42 to 58 mm for ASI + P and from 18 to 34 mm for P. No threshold was obtained for S2.1, S2.5, S3.4.2, S5.5.1, and S5.5.2. In addition, pooled weighted Spearman rank correlations (ρ) were calculated between the percentage of OF detections and event characteristics across all sites and events.

Across all precipitation events, the OF detection percentage showed significant positive correlations with precipitation intensity metrics. The strongest positive association was observed for the I_{10} ($\rho = 0.34$, $p < 0.001$), followed by I_{mean} ($\rho = 0.28$, $p = 0.005$), as shown in Table 2. By contrast, ASI exhibited a significant negative correlation with OF detection percentage ($\rho = -0.39$, $p < 0.001$), indicating lower OF detection during events preceded by wetter conditions.

In contrast, the combined index ASI + P showed only a weak and non–significant association ($\rho = -0.16$, $p = 0.13$), while P was not significantly correlated with OF detection percentage ($\rho = -0.08$, $p = 0.45$).

Restricting the analysis to wet events (ASI + P ≥ 42 mm) yielded comparable patterns. OF detection percentage remained positively correlated with precipitation intensity, with I_{10} (ρ = 0.34, $p = 0.009$) and I_{mean} ($\rho = 0.37$, $p = 0.005$) showing statistically significant relationships. At the same time, the negative association with ASI persisted ($\rho = -0.40$, $p = 0.002$), whereas P and ASI + P showed no significant correlations under wet–event conditions (Table 2).

Table 2 Pooled weighted Spearman rank correlations (ρ) between the percentage of sensors per site that detected OF and precipitation event characteristics (ASI, ASI + P, I_{10}, I_{mean}, P as defined in Section 3.7.1), shown separately for all precipitation events and for wet events (ASI + P ≥ 42 mm). Correlations were computed across all site–event combinations. The table reports Spearman's correlation coefficient (ρ), the associated p-value, and the number of site–event combinations (n).

	ASI	**ASI + P**	**I_{10}**	**I_{mean}**	**P**
All					
ρ	−0.39	−0.16	0.34	0.28	−0.08
p−value	< 0.001	0.13	< 0.001	0.005	0.45
n	105	105	105	105	105
Wet					
ρ	−0.40	0.02	0.34	0.37	0.02
p−value	0.002	0.89	0.009	0.005	0.89
n	64	64	64	64	64

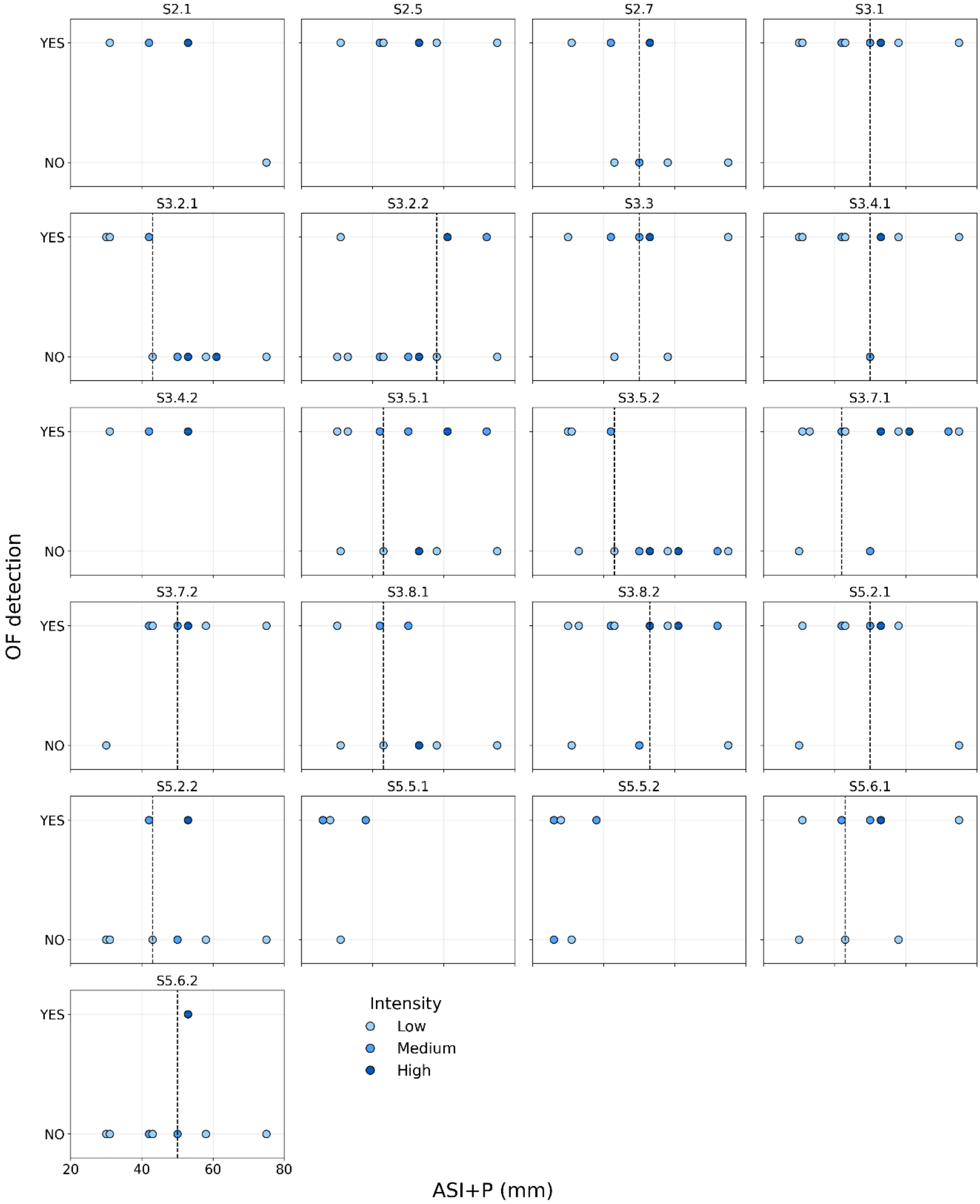

Figure 15 Relation between OF detection and ASI + P (mm) for each logger. Symbols represent individual precipitation events; color–coded by I_{mean} class (light blue = low, blue = medium, dark blue = high); dashed black lines indicate logger specific OF thresholds where identified.

4.4.3 Spatial relationship

Pooled Spearman rank correlations were computed to examine the relationship between OF detection percentage and static site characteristics. All site–event combinations were analyzed jointly, such that each site contributed multiple observations associated with different precipitation events. The OF detection percentage was defined as the proportion of sensors installed at a site that detected OF during a given event. Since organic matter (OM) was not measured at site S2.7, the number of site–event combinations (n) were reduced for analyses involving this variable.

Across all precipitation events, correlations between OF detection percentage and site characteristics were weak and statistically non–significant (Table 3). Correlation coefficients ranged from 0.02 for OM to −0.12 for vegetation, while slope ($\rho = -0.11$) and TWI ($\rho = 0.07$) likewise showed only weak associations. When the analysis was restricted to wet events, similarly small coefficients were obtained, ranging from 0.05 for OM to −0.10 for vegetation, with slope ($\rho = -0.10$) and TWI ($\rho = 0.13$) again showing no significant relationships. Overall, none of the site characteristics exhibited a consistent monotonic relationship with OF detection percentage under either all–event or wet–event conditions.

Because vegetation type represents a nominal categorical variable, differences in OF detection percentage among vegetation classes were additionally evaluated using a non–parametric Kruskal–Wallis test. This analysis likewise indicated no significant differences between vegetation classes (Kruskal–Wallis $H = 5.96$, $p = 0.11$), corroborating the results of the pooled correlation analysis.

Table 3 Pooled Spearman rank correlations (ρ) between OF detection percentage and site characteristics (OM (%), slope (°), TWI, and vegetation type as defined in Section 3.6) for all precipitation events and for wet events (ASI + P ≥ 42 mm). Correlations were computed across all site–event combinations. The table reports Spearman's correlation coefficient (ρ), the associated p–value, and the number of site–event combinations (*n*).

	OM	Slope	TWI	Vegetation
All				
ρ	0.02	−0.11	0.07	−0.12
p–value	0.88	0.30	0.49	0.26
n	98	105	105	105
Wet				
ρ	0.05	−0.10	0.13	−0.10
p–value	0.71	0.45	0.34	0.44
n	59	64	64	64

5. Discussion

5.1 Event responses

The response of OF to changes in precipitation intensity was quick (Figure 10 & 11) and synchronous for the different sites, indicating the rapid but also relatively wide onset of OF. During event 11, all active loggers responded to the first precipitation peak at 16:40 (6 mm in 30 min) and to the second peak at 19:00 (3.5 mm in 30 min), confirming the near–instantaneous initiation of OF, as also observed during the water pulse experiments on these plots by Leuteritz et al. (in review). During event 9, only the single precipitation peak at 17:10 (7.1 mm in 30 min) produced an equally immediate OF response at almost all sites. This aligns with the threshold–type behavior of OF, as reported by Gauthier et al. (2025) for the runoff plots and as also observed in streamflow within alpine catchments (Penna et al., 2011). During subsequent, weaker precipitation pulses, OF occurred only at a subset of sites, reflecting the contraction of active flow zones as precipitation intensity declined.

OF was not only detected at the onset of precipitation, but the abrupt decline in ER in both observation fields, OF1 and OF2, also coincided with the runoff plot response, thereby reflecting the direct coupling between precipitation driven OF and the sensor signal (Figure 10 & 11). Following the precipitation peaks, runoff plot decreased gradually, while ER values returned to baseline levels. Consequently, the close temporal correspondence between the two signals confirms that the ER sensors reliably captured the timing of the flow (Assendelft & van Meerveld, 2019).

Across all sites and events, the median difference between the onset of OF at the runoff plots and the ER sensors was smaller than the temporal resolution of the sensors (2 min), indicating a very close temporal correspondence. At the same time, the mean difference was 22 min, suggesting that ER sensors tended to detect OF slightly earlier than the runoff plots (Figure 14). This close agreement in detection timing indicates that both methods capture the onset of near–surface flow under similar hydrometeorological conditions, while relying on different measurement principles, with runoff plots quantifying discharge and ER sensors indicating the presence of surface wetting. Small deviations in detection timing likely reflect site–specific conditions and fine–scale spatial variability, as the ER sensors and runoff plot measurements were installed approximately 6 m apart and may therefore have sampled slightly different microtopographic positions. Variations in soil surface roughness and microtopography can influence the local initiation and routing of OF (Loos & Elsenbeer, 2011; Monger et al., 2022). In addition, minor timing differences may arise from the travel time of water from the OF gutter to the measurement point at the end of the Bernoulli tubes, or from small discrepancies in sensor clock synchronization.

The precipitation comparisons also highlight the short response times between precipitation and OF generation, with median lag times of 13 min between the onset of precipitation and OF at the plots and 12 min for the ER sensors. Such short lag times indicate that the monitored areas respond almost immediately when precipitation intensity exceeds the local infiltration capacity, leading to rapid activation of near–surface flow pathways (Dunne & Black, 1970; Zehe & Sivapalan, 2008). These short lag times agree with the short lag times for groundwater level responses in the Studibach catchment (Rinderer et al., 2016) and the quick responses observed for OF at the same plots by Gauthier et al. (2025) and Leuteritz et al. (in review). The longer mean lag times (31–51 min) suggest that delayed OF responses tend to occur during events with drier antecedent conditions, when precipitation infiltrates into available soil storage and hydrophilic soil patches before OF is initiated (Ferreira et al., 2016). However, there was no clear relationship found between TWI and OF lag times in this study.

5.2 OF occurrence

The variability in OF occurrence (as detected by the ER sensors) across sites (Figure 12) and depending on event characteristics (e.g., ASI + P values; Figure 12)) reflect the heterogeneous hydrological response of hillslopes to precipitation. The increased frequency of OF during events with higher ASI + P values, particularly for events 11, 10, and 12 (with ASI+P values of 42, 53 and 75 mm, respectively) suggests that, once the combined threshold of antecedent wetness and precipitation input was exceeded, OF occurred at a range of sites and a larger portion of the hillslope became hydrologically active. This is consistent with previous studies showing that OF areas expand with increasing precipitation totals and wetness conditions (Gauthier et al., 2025). During event 11 with an ASI + P of 42 mm, more than half of all sensors recorded OF, highlighting the wide occurrence of OF across the catchment. This is consistent with the concept of threshold dominated runoff generation, whereby the proportion of active flow areas increases sharply once a critical input level is reached (Zehe & Sivapalan, 2008). Earlier observations by Sauter (2017) using OF collectors also documented frequent OF in the Studibach catchment, supporting the conclusion that OF can be widespread and occur under relatively modest precipitation inputs.

The overall threshold for OF occurrence was 43 mm for ASI + P and 18 mm for precipitation (Figure 15). The global ASI + P threshold of 43 mm closely matches the approximate 39 mm OF threshold reported by Gauthier et al. (2025) for the same catchment and sites. The pre–cipitation threshold of 18 mm is identical to the value found by Gauthier et al. (2025) and lies within the range reported for comparable pre–Alpine catchments (Gauthier: 7–22 mm; Schneider et al., 2014: 9–21 mm). However, site–specific thresholds varied markedly, with ASI + P threshold values for the individual loggers (and thus sites) ranging from 42 to 58 mm and precipitation thresholds ranging from 18 to 34 mm. These site–specific precipitation thresholds are considerably higher than the ranges reported by Gauthier et al. (2025) and Schneider et al. (2014). A possible explanation for this is that many small precipitation events could not be evaluated because several loggers failed or produced no data during these smaller events. This means that the lower end of the threshold distribution is underrepresented in the dataset. Consequently, the thresholds primarily reflect medium to large events and thus are shifted to higher values because thresholds are only reported for loggers with a detectable breakpoint and at least seven valid events. Under these criteria, thresholds could not be determined for S2.1, S2.5, S3.4.2, S5.5.1 and S5.5.2. In most cases, there were too few valid events due to missing or unreliable sensor data, particularly during small precipitation events. This prevented the identification of a statistically robust breakpoint. This does not necessarily indicate an absence of OF at these sites but rather reflects data gaps and irregular activation patterns that limited threshold detection.

However, even under similar wetness conditions, substantial differences between sites highlight the influence of local factors, such as soil depth, microtopography and vegetation structure, on the spatial pattern of OF occurrence (Loos & Elsenbeer, 2011; Badoux et al., 2006). For example, for event 9 only one of the sensors (either OF1 or OF2) detected OF (Figure 11), suggesting that small scale differences in sensor positioning and microtopography (Zehe & Sivapalan, 2008) influence which sensor responded during this event, and that OF is thus localized.

Correlations between OF detection percentage and precipitation characteristics indicate that OF generation in the Studibach catchment is primarily controlled by precipitation characteristics rather than by cumulative wetness alone. Across all events, the strongest positive relationships were observed for short term I_{10} ($\rho = 0.34$, $p < 0.001$) and I_{mean} ($\rho = 0.28$, $p = 0.005$), whereas P ($\rho = -0.08$) and ASI + P ($\rho = -0.16$) showed only weak and statistically non–significant associations. The stronger correlation with I_{10} compared to I_{mean} suggests that brief, high intensity precipitation bursts are particularly effective in triggering OF. This pattern is consistent with an infiltration–excess runoff mechanism, as originally described by Horton (1933, 1945), and is in line with the findings of Dehotin et al. (2015), who demonstrated that runoff occurrence increases with precipitation intensity while neither precipitation intensity nor cumulative precipitation alone fully explains runoff generation.

The wet–event analysis revealed comparable but even more pronounced intensity control. In this subset, OF detection was again positively correlated with both I_{10} ($\rho = 0.34$, $p = 0.009$) and I_{mean} ($\rho = 0.37$, $p = 0.005$), while relationships with P ($\rho = 0.02$) and ASI + P ($\rho = 0.02$) were negligible and non–significant. These results further reinforce the dominance of precipitation intensity over cumulative wetness in controlling OF occurrence under wet–event conditions.

However, this intensity dominated response contrasts with the runoff plot results reported by Gauthier et al. (2025) for the same catchment. In that study, substantially stronger correlations were found between OF occurrence and P, as well as ASI + P, and a larger proportion of statistically significant relationships were reported. Given that the runoff plots were located within the same catchment, these differences are unlikely to reflect site–specific conditions alone. Instead, they likely arise from differences in event selection, sample size, and methodology. Gauthier et al. (2025) analyzed a larger number of events (27), whereas the present study was based on fewer events (16), including several with limited sensor availability. Moreover, runoff plots capture local surface responses under bounded conditions, while ER based OF detection integrates spatially heterogeneous and transient surface connectivity. As a result, cumulative precipitation and antecedent wetness may exert a stronger influence in plot–scale datasets, whereas precipitation intensity emerges as the immediate trigger of OF activation in the ER based analysis.

In contrast to the intensity metrics, ASI exhibited a consistently negative and statistically significant relationship with OF detection (all events: $\rho = -0.39$, $p < 0.001$; wet events: $\rho = -0.40$, $p = 0.002$), indicating that OF generation was favored under comparatively dry pre–event conditions. This behavior is consistent with the findings of Ferreira et al. (2016), who showed that low antecedent soil moisture can coincide with reduced infiltration capacity due to spatial variability in soil hydrophobicity, thereby promoting infiltration–excess OF even when soils are not close to saturation.

Pooled correlations between OF detection percentage and site characteristics showed no consistent spatial controls on OF occurrence across the Studibach catchment. Correlation coefficients with soil and topographic attributes were uniformly weak, ranging from $\rho = 0.02$ for organic matter to $\rho = 0.07$ for TWI, while slope and vegetation type exhibited only slight negative associations ($\rho = -0.11$ and $\rho = -0.12$, respectively). A comparable pattern was observed when the analysis was restricted to wet events. In this subset, correlation coefficients remained small for organic matter ($\rho = 0.05$), slope ($\rho = -0.10$), and vegetation type ($\rho = -0.10$), while TWI showed a slightly positive but still weak association ($\rho = 0.13$). None of these relationships were statistically significant, indicating that the percentage of OF detections was not systematically related to static site characteristics under either all–event or wet–event conditions. Taken together, these results suggest that OF occurrence at the event scale is more strongly influenced by dynamic event characteristics than by persistent spatial attributes.

However, the absence of clear spatial controls should be interpreted with caution. Although the pooled site–event analysis integrates multiple observations per site, it is based on a relatively limited number of precipitation events, which may reduce the ability to detect robust spatial patterns. By contrast, Gauthier et al. (2025) reported pronounced spatial variability in OF frequency within the same catchment, including strong positive correlations for TWI and vegetation type derived from runoff plot observations. The lack of comparable relationships in the ER based dataset likely reflects methodological differences, as ER based OF detection integrates transient surface connectivity and event–specific responses. Consequently, persistent spatial controls that are more readily identified in bounded, plot–scale experiments may be masked when OF is inferred from event–scale ER signals.

5.3 Advantages and disadvantages of ER sensors to monitor OF

The number of usable events for which OF was detected and the spatial completeness of the dataset were strongly influenced by sensor reliability. Despite some sensors failing, more than 70 % produced usable data throughout the monitoring period, indicating that the network was sufficiently robust to capture the temporal and spatial variation in OF dynamics. This is consistent with the findings of Assendelft and van Meerveld (2019), who demonstrated that low cost ER sensors can reliably detect flow timing in distributed field settings. However, the large proportion of "no data" records (57 %) reflect common causes of sensor failure, including battery depletion, moisture intrusion and interruptions in data logging, which are known limitations of environmental sensor deployments (Bhamjee & Lindsay, 2011; Campbell et al., 2013; Jones et al., 2017). Some of these issues could have been avoided with some additional "care" in the field.

Comparing the results of the two sensors, OF1 and OF2, at individual sites in Figure 9 provides additional insight into data quality. At the same time, small–scale microtopographic differences can also influence whether runoff reaches the gap in the metal plate, which helps to explain why paired sensors at the same site sometimes respond differently. When considering all valid logger–level comparisons, for example at S3.2.1, OF1 and OF2 showed matching OF classifications in 26 % of cases and differed in 15 % of cases. In the remaining 59 % of cases, however, evaluation was not possible because only one channel returned usable data.

Overall, this pattern indicates that partial data loss, rather than systematic inconsistencies between the sensors, represented the primary limitation at the logger level. Where inconsistencies did occur, they may have resulted either from logger–related issues or from genuine small–scale spatial variability in the occurrence of OF. This sensitivity to installation and local conditions, including rocky substrates, is consistent with previous findings for ER sensors (Bhamjee et al., 2016).

At the site scale, for example at S3.2, OF classifications were more coherent because the responses from all sensors installed at a given site were evaluated together. This approach integrates measurements from all loggers and their paired sensors, such as OF1 and OF2 from S3.2.1 and S3.2.2, which sample slightly different microtopographic conditions. By applying a majority–rule approach to derive a single site–level OF classification for each event, the sensors agreed in 53 % of cases and disagreed in only 12 % of cases. In the remaining 35 % of cases, however, comparison was not possible because only one sensor returned usable measurements and therefore insufficient valid data were available.

This higher level of agreement at the site scale indicates that aggregating sensor responses reduces the influence of individual sensor malfunctions and small–scale heterogeneity. Consequently, the dominant hydrological behavior of a site can be identified more robustly. Overall, these results show that although individual sensors occasionally behaved inconsistently or produced incomplete data, the prevailing OF response at the site scale was captured reliably. This finding is consistent with earlier studies demonstrating that distributed, low cost ER sensor networks can detect spatial patterns of shallow flow under field conditions (Assendelft & Van Meerveld, 2019; Bhamjee et al., 2016).

Nevertheless, substantial differences between sensors were also observed. For instance, at S3.4, OF1 showed greater variability and a higher overall resistance than OF2. This difference can be attributed to small–scale factors such as microtopography, which influence local flow concentration (Zehe & Sivapalan, 2008). At the same time, part of this discrepancy may also be related to differences in sensor construction, minor variations in sensor behavior, or sensor drift, which can occur as components age or deteriorate over time (Campbell et al., 2013). By contrast, at S5.6, both sensors displayed nearly identical patterns with smaller amplitude changes, which suggests consistent sensor behavior and more uniform flow conditions across the site.

Taken together, these results confirm the strong correlation between runoff plots and ER and therefore highlight the suitability of ER sensors for detecting both the onset and the temporal dynamics of OF under field conditions. In addition, ER sensors provide several practical advantages for monitoring ephemeral OF in heterogeneous terrain. Due to their low cost and simple construction, they can be installed at much higher spatial densities and require substantially less effort for installation than runoff plots, which involve extensive excavation, hardware installation, and on–site maintenance (Gauthier et al., 2025).

Moreover, ER sensors are particularly well suited to capturing rapid, intensity–driven responses during short precipitation pulses because the high temporal resolution of ER measurements allows the onset and recession of flow to be identified precisely. Unlike OF collectors, which must be manually emptied after each event and therefore provide only event–level information (Sauter, 2017), ER sensors operate continuously and automatically. Consequently, detailed temporal flow dynamics can be tracked without the need for servicing after each event.

Furthermore, the simple and robust design of ER sensors allows installation directly at, or slightly above or below, the soil surface and requires only minimal analytical processing, which makes them attractive for distributed hydrological monitoring (Blasch et al., 2002). Additionally, the deployment of paired sensors enhances reliability because it enables inconsistencies caused by noise or drift to be detected (Bhamjee et al., 2016; Assendelft & van Meerveld, 2019). Although data logger failures can occur in long term field deployments, more than 70 % of loggers produced usable data. This outcome is consistent with the high accuracy reported for ER sensor systems, where wet and dry classification exceeded 99 % and correctly timed transitions surpassed 90 % (Assendelft & van Meerveld, 2019).

Despite their practical benefits, ER sensors have several important limitations. The most fundamental of these is that they only provide qualitative information, distinguishing between wet and dry states rather than quantifying the amount of OF that occurs. This contrasts with runoff plots, which measure continuous discharge and provide quantitative information on flow magnitude (Gauthier et al., 2025), and OF collectors, which measure event–scale runoff volumes (though only for small amounts, Sauter, 2017).

Field deployments of ER sensors are vulnerable to battery depletion, moisture intrusion, cable damage, and logger malfunction, which can result in substantial data loss. In this study, for example, 57 % of all logger records were classified as “no data” and 28 % as “unreliable”. The considerable fraction of “unreliable” data highlights the sensitivity of ER measurements to noise. Such fluctuations are well documented in ER-based monitoring systems (Bhamjee et al., 2016; Bhamjee & Lindsay, 2011) because ER signals are prone to noise generated by ripples, damp sediment, or unstable electrode contact, which can result in short spikes, false positives, or ambiguous transitions. (Bhamjee & Lindsay, 2011; Assendelft & van Meerveld, 2019).

OF detections also depend strongly on local microtopography as small differences in placement determine whether OF reaches the electrodes. Moreover, if sensors are not positioned at the lowest point or surface morphology shifts during storms, OF may bypass the electrodes or accumulate in puddles, producing false “no–flow” or “flow” indications (Kaplan et al., 2019). Blasch et al. (2002) likewise emphasized the sensitivity of ER sensors to placement conditions and demonstrated that even minor changes in bed elevation, sediment deposition, or erosion can either bury or expose electrodes. Consequently, such alterations can lead to missed detections or to delayed drying signals. Furthermore, they found that the accumulation of fine sediments around the electrodes can influence drying behavior and shift the timing of flow termination, thereby introducing uncertainty into flow decline estimates. In addition, issues such as drift, corrosion, or cable damage may remain undetected over multiple events if sensors are not checked and maintained regularly. Overall, these limitations illustrate that although ER sensors are highly effective for identifying when OF occurs, they cannot replace quantitative methods when information on runoff magnitude is required.

The detection workflow itself also imposed several methodological constraints that affected the reliability of OF identification. The procedure relied on a sequence of threshold based filters, which were necessary to reduce noise but, at the same time, applied rigid criteria to a process that varies across sensors and sites. Overall, the multi–step detection workflow required substantial manual effort, including repeated adjustments, visual inspections, and quality control, to isolate reliable OF signals from noise and sensor artefacts. In particular, the drop–detection rule prioritizes abrupt declines in resistance, such that OF associated with gradual surface wetting and slowly developing flow paths, most commonly during low intensity precipitation events, is likely to remain undetected. Likewise, the percentile–based plausibility filter may exclude genuine events when long term drift, sediment deposition, or electrode ageing modifies the sensor’s dry–state signal. In addition, event slicing can truncate responses that begin before or extend beyond the predefined analysis window.

Further rules were implemented to flag probable sensor malfunctions rather than true hydrological behavior, including the exclusion of event windows containing twelve or more consecutive identical values, as well as the removal of individual measurements of 1,000,000 or more. However, since prolonged dry periods can also occur naturally, these filters may have removed genuine OF detections in situations where valid wetting signals followed extended dry sequences. Although the 20 % drop–detection threshold could theoretically be relaxed, such an adjustment would increase the likelihood of retaining malfunctioning sensors. Consequently, some genuine OF events were likely excluded at this stage.

The detection threshold therefore had to be determined manually through repeated adjustment and visual verification of the resulting detections. If the threshold was set too high, many real OF signals failed to satisfy the 20 % drop criterion and were therefore missed. Conversely, if it was set too low, numerous false positives were generated, reflecting noise rather than hydrological responses.

In addition, the reliability of the method depends on the availability of complete time series, as missing or unreliable data disproportionately affects the detection of smaller events and lower end OF thresholds. Taken together, these factors demonstrate that, while the ER sensors accurately captured OF timing when signals were clear, the detection workflow inevitably influenced the classification of events as OF. The workflow was deliberately designed to prioritize the identification of definitive OF events, and thus applied conservative filtering criteria, which likely resulted in the omission of some genuine but less distinct OF occurrences.. These methodological limitations should therefore be considered when interpreting the results. Furthermore, it should be remembered that the method identifies the moment when water connects the electrodes rather than actual downslope flow.

5.4 Suggestions for improvements of ER sensors

Several improvements could enhance the reliability of ER based OF monitoring. One challenge in this study was that ER sensors could not distinguish between standing and flowing water. However, Assendelft and van Meerveld (2019) demonstrated that ER sensors in intermittent streams can detect the wet/dry state exceptionally accurately (99.9 % of states correctly identified) and achieve very high timing accuracy (93.5 %). This explains why the initial OF onset was captured so well in this study. However, once the initial wetting pulse has passed, ER sensors cannot confirm whether water is flowing or present as standing water or residual moisture. Considering the performance of all the sensor types tested by Assendelft and van Meerveld (2019) and Bhamjee and Lindsay (2011), the optimal solution would be to combine an ER sensor with a simple flow sensor, as this pairing provides reliable information on water presence and confirms actual flow. Integrating a flow detector of this kind into the metal plate gap could therefore help to distinguish between flowing and non–flowing conditions, thereby reducing post–onset uncertainty. However, Assendelft and van Meerveld (2019) also showed for their sensors that there was a minimum amount of flow needed for the flow sensor to record data.

Consequently, the combined approach is most effective for identifying clearly developed OF with sustained flow, whereas slowly moving or very shallow flow, may still remain indistinguishable. Thus, the sensor combination improves OF classification for a subset of events but does not fully resolve ambiguities under low–flow conditions.

To improve the affordability and spatial coverage of OF detection, multiple sensors can be attached to a single logger. Bhamjee and Lindsay (2011) highlighted that this configuration is cost–efficient and increases the spatial resolution of the data. However, concentrating several sensors on one logger also increases vulnerability, because a single logger failure results in the simultaneous loss of multiple sensor records and shared memory capacity is exhausted more quickly than when sensors operate on dedicated loggers. This trade–off was evident in this study, where logger failures removed entire sensor sets during several events. Therefore, despite the higher initial costs, distributing sensors across a larger number of loggers or increasing the logger–to–sensor ratio is recommended, as this approach improves redundancy and reduces the likelihood that complete events are represented by only a single operational sensor.

The installation design could be further refined. As Goulsbra et al. (2009) emphasized, reliable and high quality data depend strongly on careful routine maintenance and well–chosen monitoring locations. In addition, Blasch et al. (2002) and Kaplan et al. (2019) showed that even small differences in microtopography, sediment accumulation, and sensor placement can substantially affect whether intermittent streamflow reaches a detector. For this reason, small–scale irrigation tests prior to installation, together with the placement of several ER sensors in slightly different microtopographic positions, would increase the likelihood that at least one sensor is positioned along an active OF flow path.

Moreover, Bhamjee and Lindsay (2011) demonstrated that state loggers, which record only when a change occurs, avoid the memory limitations associated with interval logging and remove the need to determine sensor–specific resistance thresholds. In the context of this study, replacing the fixed 20 % drop–detection threshold with sensor–specific or dynamically derived thresholds would likewise reduce subjectivity and improve consistency between loggers. Since state loggers use predetermined, constant internal cutoffs to classify ‘open’ and ‘closed’ states, they eliminate the need for calibration when relative resistance values are used and therefore support more standardized transition detection.

The clear offset between OF1 and OF2 reflects that the sensors were not individually calibrated and therefore operated on different resistance scales. At the same time, additional variation in electrode geometry, installation contact, and microtopography further contributes to these discrepancies. Consequently, applying a state–logging approach to ER based OF monitoring could simplify calibration, extend logging duration, and produce clearer transition signals, while also reducing false positives caused by noise. However, state loggers do not provide raw sensor data, which restricts the ability to clean measurements, apply site–specific corrections, or identify sensor errors. As a result, the quality and interpretability of the resulting state data are more limited than in interval logging (Assendelft & van Meerveld, 2019).

Finally, long term data availability could be improved through better hardware reliability and more consistent field maintenance. In particular, more frequent field checks, improved waterproofing and enhanced power management would be beneficial. Assendelft and van Meerveld (2019) demonstrated that multi–sensor systems can operate for nine months on four lithium AA batteries with appropriate power–saving measures and that a more efficient voltage regulator would further reduce energy consumption. A future setup could therefore combine rechargeable batteries with small, low cost solar panels, which could help extend deployment durations. However, the effectiveness of such a system would likely depend on canopy cover and local light availability, and reliable operation in forested settings cannot be assumed without site–specific testing. In this study, there was only one operational logger for several events (4−8). Although loggers were deployed for 21 potential events, only 16 were usable due to battery depletion and hardware failure.

6. Conclusion

This study evaluated the usefulness of low cost ER sensors in detecting OF and examined the relationship between OF occurrence and selected event and site characteristics in the Studibach catchment. By comparing ER sensor data with runoff plot measurements and relating OF detection to precipitation characteristics and site properties, the study provides a complementary perspective on hydrological processes and the performance of ER based OF detection methods.

ER sensors proved to be highly effective in detecting the timing of OF initiation. Across all site–event combinations, the onset of OF identified by ER sensors closely aligned with runoff plot responses measured at the plots, with median and mean time differences of 2 and 22 min, respectively. These small differences suggest that ER sensors can reliably capture the rapid, event–driven initiation of OF, particularly during short, intense bursts of precipitation. While runoff plots provide quantitative discharge measurements, ER sensors capture surface wetting and connectivity. This makes the two methods complementary rather than interchangeable.

Within individual measurement sites, ER sensors did not always exhibit identical detection behavior when evaluated individually. At the logger level, OF classifications agreed in 26 % of comparable events and disagreed in 15 %, while in 59 % of cases, only one sensor provided usable data, preventing direct comparison. These discrepancies were primarily caused by partial data loss due to battery depletion or hardware failure, as well as by small scale microtopographic variability affecting local flow paths. Aggregating sensor responses at the site scale using a majority–rule approach made OF detection markedly more coherent: agreement increased to 53 %, disagreement was reduced to 12 %, and limited sensor availability affected the remaining 35 % of events. This demonstrates that site–level aggregation substantially improves the robustness of ER based OF classification.

The occurrence of OF in the Studibach catchment was primarily controlled by event characteristics rather than static site properties. Short term precipitation intensity exhibited the strongest correlation with OF detection, with I_{10} reaching correlation coefficients of up to 0.34. I_{mean} exhibited a weaker correlation. In contrast, P and ASI + P exhibited only weak, non–significant relationships with OF occurrence. There was a consistently negative relationship ($\rho \approx -0.39$) between ASI and OF detection, suggesting that infiltration–excess processes were dominant and were likely linked to reduced infiltration capacity under relatively dry pre–event conditions. Pooled correlations with site characteristics, such as TWI, slope, vegetation type and OM, remained weak and non–significant. This indicates that event–scale forcing outweighs persistent spatial controls in the ER based dataset.

Sensor availability was a significant limitation of the monitoring setup. Although ER loggers were deployed for 21 potential precipitation events, only 16 events were fully usable due to battery depletion and hardware failure. During events 4–8, only one logger was operational, which strongly limited spatial comparability. Overall, 72 % of the deployed loggers provided usable data over the study period, demonstrating reasonable, though not complete, system reliability. This uneven data coverage likely reduced statistical power and may have contributed to the apparent dominance of high intensity responses and the negative relationship with antecedent soil moisture. Recognizing this limitation means that the ER based results should be considered as conservative estimates of OF occurrence rather than exhaustive representations.

Overall, this study shows that ER sensors are a reliable and practical way of monitoring the timing and location of OF in varied, pre–Alpine terrain. While they cannot quantify runoff volumes and remain sensitive to installation quality and data gaps, their low cost, high temporal resolution and scalability make them particularly valuable for the distributed monitoring of ephemeral OF processes. Combined with aggregation strategies and complementary quantitative methods, such as runoff plots, ER sensors have strong potential to improve understanding of hillslope runoff connectivity and event–scale hydrological dynamics.

Language support tools (ChatGPT, OpenAI) were used exclusively for grammatical and stylistic revision. The scientific content, data analysis, interpretation of results, and conclusions were developed independently by the author.

7. References

Abrahams, A. D., Parsons, A. J., & Wainwright, J. (1994). Resistance to overland flow on semiarid grassland and shrubland hillslopes, Walnut Gulch, southern Arizona. *Journal of Hydrology*, *156*(1-4), 431-446. https://doi.org/10.1016/0022-1694(94)90088-4

Assendelft, R., & van Meerveld, H. J. (2019). A Low-Cost, Multi-Sensor System to Monitor Temporary Stream Dynamics in Mountainous Headwater Catchments. *Sensors*, *19*(21), 4645. https://doi.org/10.3390/s19214645

Badoux, A., Witzig, J., Germann, P. F., Kienholz, H., Lüscher, P., Weingartner, R., & Hegg, C. (2006). Investigations on the runoff generation at the profile and plot scales, Swiss Emmental. *Hydrological Processes*, *20*(2), 377-394. https://doi.org/10.1002/hyp.6056

Bayard, D., Stähli, M., Parriaux, A., & Flühler, H. (2005). The influence of seasonally frozen soil on the snowmelt runoff at two Alpine sites in southern Switzerland. *Journal of Hydrology*, *309*(1-4), 66-84. https://doi.org/10.1016/j.jhydrol.2004.11.012

Beven, K. J., & Kirkby, M. J. (1979). A physically based, variable contributing area model of basin hydrology / Un modèle à base physique de zone d'appel variable de l'hydrologie du bassin versant. *Hydrological Sciences Bulletin*, *24*(1), 43-69. https://doi.org/10.1080/02626667909491834

Bhamjee, R., & Lindsay, J. B. (2011). Ephemeral stream sensor design using state loggers. *Hydrology and Earth System Sciences*, *15*(3), 1009-1021. https://doi.org/10.5194/hess-15-1009-2011

Bhamjee, R., Lindsay, J. B., & Cockburn, J. (2016). Monitoring ephemeral headwater streams: A paired-sensor approach: Monitoring Ephemeral Headwater Streams: A Paired-sensor Approach. *Hydrological Processes*, *30*(6), 888-898. https://doi.org/10.1002/hyp.10677

Blasch, K. W., Ferré, T. P. A., Christensen, A. H., & Hoffmann, J. P. (2002). New Field Method to Determine Streamflow Timing Using Electrical Resistance Sensors. *Vadose Zone Journal*, *1*(2), 289-299. https://doi.org/10.2136/vzj2002.2890

Blasch, K. W., Ferré, T. P. A., & Hoffmann, J. P. (2004). A Statistical Technique for Interpreting Streamflow Timing Using Streambed Sediment Thermographs. *Vadose Zone Journal*, *3*(3), 936-946. https://doi.org/10.2136/vzj2004.0936

Buda, A. R., Kleinman, P. J. A., Srinivasan, M. S., Bryant, R. B., & Feyereisen, G. W. (2009). Factors influencing surface runoff generation from two agricultural hillslopes in central Pennsylvania. *Hydrological Processes*, *23*(9), 1295-1312. https://doi.org/10.1002/hyp.7237

Bujak-Ozga, I., Von Freyberg, J., Zimmer, M., Rinaldo, A., Benettin, P., & Van Meerveld, I. (2024). Changes in flowing drainage network and stream chemistry during rainfall events for two pre-Alpine catchments. *Hydrology and Earth System Sciences*, *29*(11), 2339-2359 https://doi.org/10.5194/hess-2024-67

Campbell, J. L., Rustad, L. E., Porter, J. H., Taylor, J. R., Dereszynski, E. W., Shanley, J. B., Gries, C., Henshaw, D. L., Martin, M. E., Sheldon, W. M., & Boose, E. R. (2013). Quantity is Nothing without Quality: Automated QA/QC for Streaming Environmental Sensor Data. *BioScience*, *63*(7), 574-585. https://doi.org/10.1525/bio.2013.63.7.10

Casanova, M., Messing, I., & Joel, A. (2000). Influence of aspect and slope gradient on hydraulic conductivity measured by tension infiltrometer. *Hydrological Processes*, *14*(1), 155-164. https://doi.org/10.1002/%28SICI%291099-1085%28200001%2914%3A1%3C155%3A%3AAID-HYP917%3E3.0.CO%3B2-J

Chaves, J. E., Neill, C., & Germer, S. (2009). Nitrogen Transformations in Flowpaths Leading from Soils to Streams in Amazon Forest and Pasture. *Ecosystems*, *12*, 961-972. https://doi.org/10.1007/s10021-009-9270-4

Constantz, J., Stonestorm, D., Stewart, A. E., Niswonger, R., & Smith, T. R. (2001). Analysis of streambed temperatures in ephemeral channels to determine streamflow frequency and duration. *Water Resources Research*, *37*(2), 317-328. https://doi.org/10.1029/2000WR900271

de Jong, S. M., Heijenk, R. A., Nijland, W., & van der Meijde, M. (2020). Monitoring Soil Moisture Dynamics Using Electrical Resistivity Tomography under Homogeneous Field Conditions. *Sensors*, *20*(18), Article 18. https://doi.org/10.3390/s20185313

Dehotin, J., Breil, P., Braud, I., De Lavenne, A., Lagouy, M., & Sarrazin, B. (2015). Detecting surface runoff location in a small catchment using distributed and simple observation method. *Journal of Hydrology*, *525*, 113-129. https://doi.org/10.1016/j.jhydrol.2015.02.051

Detty, J. M., & McGuire, K. J. (2010). Threshold changes in storm runoff generation at a till-mantled headwater catchment. *Water Resources Research*, *46*(7), 2009WR008102. https://doi.org/10.1029/2009WR008102

Dunne, T., & Black, R. D. (1970). Partial Area Contributions to Storm Runoff in a Small New England Watershed. *Water Resources Research*, *6*(5), 1296-1311. https://doi.org/10.1029/WR006i005p01296

Elsenbeer, H., & Lack, A. (1996). Hydrometric and hydrochemicai evidence for fast flowpaths at La Cuenca, Western Amazonia. *Journal of Hydrology*, *180*(1-4), 237-250. https://doi.org/10.1016/0022-1694(95)02889-7

Emmett, W. W. (1970). The hydraulics of overland flow on hillslopes. *Professional Paper* (Nos. 662-A). U.S. Govt. Print. Off.,. https://doi.org/10.3133/pp662A

Fang, Q., Zi, R., Zhao, L., Fan, C., Fang, F., & Qian, X. (2024). Effect of bedrock permeability on runoff and soil loss in soil-mantled karst slopes under successive rainfall conditions. *CATENA*, *247*, 108524. https://doi.org/10.1016/j.catena.2024.108524

Ferreira, C. S. S., Walsh, R. P. D., Shakesby, R. A., Keizer, J. J., Soares, D., González-Pelayo, O., Coelho, C. O. A., & Ferreira, A. J. D. (2016). Differences in overland flow, hydrophobicity and soil moisture dynamics between Mediterranean woodland types in a peri-urban catchment in Portugal. *Journal of Hydrology*, *533*, 473-485. https://doi.org/10.1016/j.jhydrol.2015.12.040

Feyen, H., Leuenberger, J., Papritz, A., Gysi, M., Flühler, H., & Schleppi, P. (1996). Runoff processes in catchments with a small scale topography. *Physics and Chemistry of the Earth*, *21*(3), 177-181. https://doi.org/10.1016/S0079-1946(97)85581-4

Fischer, B. M. C., Stähli, M., & Seibert, J. (2017). Pre-event water contributions to runoff events of different magnitude in pre-alpine headwaters. *Hydrology Research*, *48*(1), 28-47. https://doi.org/10.2166/nh.2016.176

Gascuel-Odoux, C., Cros-Cayot, S., & Durand, P. (1996). SPATIAL VARIATIONS OF SHEET FLOW AND SEDIMENT TRANSPORT ON AN AGRICULTURAL FIELD. *Earth Surface Processes and Landforms*, *21*(9), 843-851. https://doi-org.ezproxy.uzh.ch/10.1002/(SICI)1096-9837(199609)21:9<843::AID-ESP626>3.0.CO;2-I

Gauthier, V. A., Leuteritz, A., & van Meerveld, I. (2025). When and where does near-surface runoff occur in a pre-Alpine headwater catchment?. *Hydrology and Earth System Science, 29*(16), 3889-3905. https://doi.org/10.5194/hess-2024-398

Gerke, K. M., Sidle, R. C., & Mallants, D. (2015). Preferential flow mechanisms identified from staining experiments in forested hillslopes. *Hydrological Processes*, *29*(21), 4562-4578. https://doi.org/10.1002/hyp.10468

Godsey, S., Elsenbeer, H., & Stallard, R. (2004). Overland flow generation in two lithologically distinct rainforest catchments. *Journal of Hydrology*, *295*(1-4), 276-290. https://doi.org/10.1016/j.jhydrol.2004.03.014

Goulsbra, C. S., Lindsay, J. B., & Evans, M. G. (2009). A new approach to the application of electrical resistance sensors to measuring the onset of ephemeral streamflow in wetland environments. *Water Resources Research*, *45*(9). https://doi.org/10.1029/2009WR007789

Guentner, A., Uhlenbrook, S., Seibert, J., Leibundgut, C., Diekkrüger, B., Kirkby, M., & Schröder, U. (1999). Estimation of saturation excess overland flow areas: Comparison of topographic index calculations with field mapping. *International Association of Hydrological Sciences*, 203–210.

Haacke, N., & Paton, E. (2023). Impact-based classification of extreme rainfall events using a simplified overland flow model. *Urban Water Journal*, *20*(3), 330-340. https://doi.org/10.1080/1573062X.2022.2164731

Hagedorn, F., Schleppi, P., Bucher, J., & Flühler, H. (2001). Retention and Leaching of Elevated N Deposition in a Forest Ecosystem with Gleysols. *Water, Air, and Soil Pollution*, *129*, 119-142. https://doi.org/10.1023/a:1010397232239

Hagedorn, F., Schleppi, P., Waldner, P., & Flühler, H. (2000). Export of dissolved organic carbon and nitrogen from Gleysol dominated catchments - the significance of water flow paths. *Biogeochemistry*, *50*, 137-161. https://doi.org/10.1023/a:1006398105953

Hendriks, M. (2010). Introduction to Physical Hydrology. OUP Oxford.

Horton, R. E. (1933). The Role of infiltration in the hydrologic cycle. *Eos, Transactions American Geophysical Union*, *14*(1), 446-460. https://doi.org/10.1029/TR014i001p00446

Horton, R. E. (1945). Erosional development of streams and their drainage basins; hydrophysical approach to quantitative morphology. *Geological Society of America Bulletin*, *56*(3), 275. https://doi.org/10.1130/0016-7606(1945)56[275:EDOSAT]2.0.CO;2

Hu, L., Bao, W., Shi, P., Wang, J., & Lu, M. (2020). Simulation of overland flow considering the influence of topographic depressions. *Scientific Reports*, *10*, 6128. https://doi.org/10.1038/s41598-020-63001-y

Intergovernmental Panel on Climate Change. (2023). Climate change 2021 - The physical science basis. *Cambridge University Press*. https://doi.org/10.1017/9781009157896

Jaeger, K. L., & Olden, J. D. (2012). Electrical resistance sensor arrays as a means to quantify longitudinal connectivity of rivers. *River Research and Applications*, *28*(10), 1843-1852. https://doi.org/10.1002/rra.1554

Jansson, M. B., & Strömberg, K. (2004). Surface runoff and soil loss in tropical rainforest and pasture, Costa Rica, and indices explaining their variations. *Zeitschrift Für Geomorphologie*, *48*(1), 25-51. https://doi.org/10.1127/zfg/48/2004/25

Jones, A. S., Aanderud, Z. T., Horsburgh, J. S., Eiriksson, D. P., Dastrup, D., Cox, C., Jones, S. B., Bowling, D. R., Carlisle, J., Carling, G. T., & Baker, M. A. (2017). Designing and Implementing a Network for Sensing Water Quality and Hydrology across Mountain to Urban Transitions. *JAWRA Journal of the American Water Resources Association*, *53*(5), 1095-1120. https://doi.org/10.1111/1752-1688.12557

Kaplan, N. H., Sohrt, E., Blume, T., & Weiler, M. (2019). Monitoring ephemeral, intermittent and perennial streamflow: A dataset from 182 sites in the Attert catchment, Luxembourg. *Earth System Science Data*, *11*(3), 1363-1374. https://doi.org/10.5194/essd-11-1363-2019

Kiewiet, L., van Meerveld, I., Stähli, M., & Seibert, J. (2020). Do stream water solute concentrations reflect when connectivity occurs in a small, pre-Alpine headwater catchment? *Hydrology and Earth System Sciences*, *24*(7), 3381-3398. https://doi.org/10.5194/hess-24-3381-2020

Kurz, I., O'Reilly, C. D., & Tunney, H. (2006). Impact of cattle on soil physical properties and nutrient concentrations in overland flow from pasture in Ireland. *Agriculture, Ecosystems & Environment*, *113*(1-4), 378-390. https://doi.org/10.1016/j.agee.2005.10.004

Leatherman, S. P. (1987). Field Measurement of Microtopography. *Journal of Coastal Research*, *3*, 233-235.

Leuteritz, A., Gauthier, V. A., & van Meerveld, I. (in review). Tracing near-surface runoff in a pre-Alpine headwater catchment. *Preprint egusphere*. https://doi.org/10.5194/egusphere-2025-1677

Loos, M., & Elsenbeer, H. (2011). Topographic controls on overland flow generation in a forest - An ensemble tree approach. *Journal of Hydrology*, *409*(1-2), 94-103. https://doi.org/10.1016/j.jhydrol.2011.08.002

Maier, F., van Meerveld, I., & Weiler, M. (2021). Long-Term Changes in Runoff Generation Mechanisms for Two Proglacial Areas in the Swiss Alps II: Subsurface Flow. *Water Resources Research*, *57*(12), e2021WR030223. https://doi.org/10.1029/2021WR030223

Masselink, R. J. H., Heckmann, T., Temme, A. J. A. M., Anders, N. S., Gooren, H. P. A., & Keesstra, S. D. (2017). A network theory approach for a better understanding of overland flow connectivity. *Hydrological Processes*, *31*(1), 207-220. https://doi.org/10.1002/hyp.10993

Megahan, W. F. (1983). Hydrologic effects of clearcutting and wildfire on steep granitic slopes in Idaho. *Water Resources Research*, *19*(3), 811-819. https://doi.org/10.1029/WR019i003p00811

Mishra, P. K., Rai, A., Abdelrahman, K., Rai, S. C., & Tiwari, A. (2022). Land Degradation, Overland Flow, Soil Erosion, and Nutrient Loss in the Eastern Himalayas, India. *Land*, *11*(2), 179. https://doi.org/10.3390/land11020179

Mohn, J., Schürmann, A., Hagedorn, F., Schleppi, P., & Bachofen, R. (2000). Increased rates of denitrification in nitrogen-treated forest soils. *Forest Ecology and Management*, *137*(1-3*)*, 113-119. https://doi-org.ezproxy.uzh.ch/10.1016/S0378-1127(99)00320-5

Monger, F., Bond, S., Spracklen, D. V., & Kirkby, M. J. (2022). Overland flow velocity and soil properties in established semi-natural woodland and wood pasture in an upland catchment. *Hydrological Processes*, *36*(4), e14567. https://doi.org/10.1002/hyp.14567

Moody, J. A., & Martin, R. G. (2015). Measurements of the initiation of post-wildfire runoff during rainstorms using *in situ* overland flow detectors. *Earth Surface Processes and Landforms*, *40*(8), 1043-1056. https://doi.org/10.1002/esp.3704

Mounirou, L. A., Yacouba, H., Karambiri, H., Paturel, J.-E., & Mahé, G. (2012). Measuring runoff by plots at different scales: Understanding and analysing the sources of variation. *Comptes Rendus. Géoscience*, *344*(9), 441-448. https://doi.org/10.1016/j.crte.2012.08.004

Pachepsky, Ya. A., Timlin, D. J., & Rawls, W. J. (2001). Soil Water Retention as Related to Topographic Variables. *Soil Science Society of America Journal*, *65*(6), 1787-1795. https://doi.org/10.2136/sssaj2001.1787

Penna, D., Tromp-van Meerveld, H. J., Gobbi, A., Borga, M., & Dalla Fontana, G. (2011). The influence of soil moisture on threshold runoff generation processes in an alpine headwater catchment. *Hydrology and Earth System Sciences*, *15*(3), 689-702. https://doi.org/10.5194/hess-15-689-2011

Pietola, L., Horn, R., & Yli-Halla, M. (2005). Effects of trampling by cattle on the hydraulic and mechanical properties of soil. *Soil and Tillage Research*, *82*(1), 99-108. https://doi.org/10.1016/j.still.2004.08.004

Reaney, S. M., Bracken, L. J., & Kirkby, M. J. (2014). The importance of surface controls on overland flow connectivity in semi-arid environments: Results from a numerical experimental approach. *Hydrological Processes*, *28*(4), 2116-2128. https://doi.org/10.1002/hyp.9769

Rinderer, M., van Meerveld, H. J., & Seibert, J. (2014). Topographic controls on shallow groundwater levels in a steep, prealpine catchment: When are the TWI assumptions valid? *Water Resources Research*, *50*(7), 6067-6080. https://doi.org/10.1002/2013wr015009

Rinderer, M., van Meerveld, I., Stähli, M., & Seibert, J. (2016). Is groundwater response timing in a pre-alpine catchment controlled more by topography or by rainfall? *Hydrological Processes*, *30*(7), 1036-1051. https://doi.org/10.1002/hyp.10634

Sauter, T. (2017). Occurrence and Chemical Composition of Overland Flow in a Pre-alpine catchment, Alptal (CH). *University of Zurich*, 87.

Schallner, J. W., Johnson, J. C., Williams, C. J., & Ganguli, A. C. (2021). Evaluation of a Runoff Monitoring Methodology for Rangelands: UBeTubes. *Rangeland Ecology & Management*, *78*, 46-50. https://doi.org/10.1016/j.rama.2021.05.003

Scherrer, S. (1996). Abflussbildung bei Starkniederschlägen: Identifikation von Abflussprozessen mittels künstlicher Niederschläge. *ETH Zurich.* https://doi.org/10.3929/ETHZ-A-001735502

Scherrer, S., Naef, F., Faeh, A. O., & Cordery, I. (2007). Formation of runoff at the hillslope scale during intense precipitation. *Hydrology and Earth System Sciences*, *11*(2), 907-922. https://doi.org/10.5194/hess-11-907-2007

Schleppi, P., Muller, N., Feyen, H., Papritz, A., Bucher, J. B., & Flühler, H. (1998). Nitrogen budgets of two small experimental forested catchments at Alptal, Switzerland. *Forest Ecology and Management*, *101*(1-3), 177-185. https://doi.org/10.1016/s0378-1127(97)00134-5

Schneider, P., Pool, S., Strouhal, L., & Seibert, J. (2014). True colors - experimental identification of hydrological processes at a hillslope prone to slide. *Hydrology and Earth System Sciences*, *18*(2), 875-892. https://doi.org/10.5194/hess-18-875-2014

Srinivasan, M. S., Gburek, W. J., & Hamlett, J. M. (2002). Dynamics of stormflow generation—A hillslope-scale field study in east-central Pennsylvania, USA. *Hydrological Processes*, *16*(3), 649-665. https://doi.org/10.1002/hyp.311

Stähli, M., & Gustafsson, D. (2006). Long-term investigations of the snow cover in a subalpine semi-forested catchment. *Hydrological Processes*, *20*(2), 411-428. https://doi.org/10.1002/hyp.6058

Stewart, R. D., Liu, Z., Rupp, D. E., Higgins, C. W., & Selker, J. S. (2015). A new instrument to measure plot-scale runoff. *Geoscientific Instrumentation, Methods and Data Systems*, *4*(1), 57-64. https://doi.org/10.5194/gi-4-57-2015

Tarboton, D. G. (2003). Rainfall-Runoff Processes. *Utah State University*, 159.

van Meerveld, H. J. I., Kirchner, J. W., Vis, M. J. P., Assendelft, R. S., & Seibert, J. (2019). Expansion and contraction of the flowing stream network alter hillslope flowpath lengths and the shape of the travel time distribution. *Hydrology and Earth System Sciences*, *23*(11), 4825-4834. https://doi.org/10.5194/hess-23-4825-2019

Vigiak, O., Van Dijck, S. J. E., Van Loon, E. E., & Stroosnijder, L. (2006). Matching hydrologic response to measured effective hydraulic conductivity. *Hydrological Processes*, *20*(3), 487-504. https://doi.org/10.1002/hyp.5916

von Freyberg, J., Studer, B., Rinderer, M., & Kirchner, J. W. (2018). Studying catchment storm response using event- and pre-event-water volumes as fractions of precipitation rather than discharge. *Hydrology and Earth System Sciences*, *22*(11), 5847-5865. https://doi.org/10.5194/hess-22-5847-2018

Wainwright, J., & Parsons, A. J. (2002). The effect of temporal variations in rainfall on scale dependency in runoff coefficients. *Water Resources Research*, *38*(12), 7-1-7-10. https://doi.org/10.1029/2000WR000188

Wainwright, J., Parsons, A. J., & Abrahams, A. D. (2000). Plot-scale studies of vegetation, overland flow and erosion interactions: Case studies from Arizona and New Mexico. *Hydrological Processes*, *14*(16-17), 2921-2943. https://doi-org.ezproxy.uzh.ch/10.1002/1099-1085(200011/12)14:16/17<2921::AID-HYP127>3.0.CO;2-7

Weiler, M., & Naef, F. (1998). Study of runoff generation on hillslopes using tracer experiments and a physically based numerical hillslope model. *IAHS Publication*, *248*, 353-360.

Weiler, M., & Naef, F. (2003). An experimental tracer study of the role of macropores in infiltration in grassland soils. *Hydrological Processes*, *17*(2), 477-493. https://doi.org/10.1002/hyp.1136

Weiler, M., Scherrer, S., Naef, F., & Burlando, P. (1999). Hydrograph separation of runoff components based on measuring hydraulic state variables, tracer experiments, and weighting methods. *IAHS Publications*, *258*, 249-255.

Wierda, A., Veen, A. W. L., & Hutjes, R. W. A. (1989). Infiltration at the Tai rain forest (Ivory Coast): Measurements and modelling. *Hydrological Processes*, *3*(4), 371-382. https://doi.org/10.1002/hyp.3360030408

Wilcox, B. P., Wilding, L. P., & Woodruff, C. M. (2007). Soil and topographic controls on runoff generation from stepped landforms in the Edwards Plateau of Central Texas. *Geophysical Research Letters*, *34*(24), 2007GL030860. https://doi.org/10.1029/2007GL030860

Yen, B. C., & Akan, A. O. (1983). EFFECTS OF SOIL PROPERTIES ON OVERLAND FLOW AND INFILTRATION. *Journal of Hydraulic Research*, *21*(2), 153-173. https://doi.org/10.1080/00221688309499442

Zehe, E., & Sivapalan, M. (2008). Threshold behavior in hydrological systems and geo-ecosystems: Manifestations, controls and implications for predictability. *Hydrology and Earth System Sciences, 13*(7), 1273-1297. https://doi.org/10.5194/hessd-5-3247-2008

Ziegler, A. D., Giambelluca, T. W., Sutherland, R. A., Vana, T. T., & Nullet, M. A. (2001). Horton overland flow contribution to runoff on unpaved mountain roads: A case study in northern Thailand. *Hydrological Processes*, *15*(16), 3203-3208. https://doi.org/10.1002/hyp.480

Zimmermann, A., Schinn, D. S., Francke, T., Elsenbeer, H., & Zimmermann, B. (2013). Uncovering patterns of near-surface saturated hydraulic conductivity in an overland flow-controlled landscape. *Geoderma*, *195-196*, 1-11. https://doi.org/10.1016/j.geoderma.2012.11.002

Zimmermann, B., Zimmermann, A., Turner, B. L., Francke, T., & Elsenbeer, H. (2014). Connectivity of overland flow by drainage network expansion in a rain forest catchment: Connectivity of overland flow in a rainforest catchment. *Water Resources Research*, *50*(2), 1457-1473. https://doi.org/10.1002/2012WR012660

Zwartendijk, B. W., Van Meerveld, H. J., Ghimire, C. P., Ravelona, M., Lahitiana, J., & Bruijnzeel, L. A. (2020). Soil water- and overland flow dynamics in a tropical catchment subject to long-term slash-and-burn agriculture. *Journal of Hydrology*, *582*, 124287. https://doi.org/10.1016/j.jhydrol.2019.124287

Table of Figures

List of Tables

Appendix A: Precipitation events

Table 1 Overview of precipitation events and associated characteristics.

EventID	Date	P	I_{10}	I_{mean}	I_{class}	D	ASI	ASI+P
-	dd/mm/yy	(mm)	(mm/h)	(mm/h)	-	(hh:min)	(mm)	(mm)
1	24.06.2022	38	63	5.4	High	05:35	23	61
2	27.06.2022	10	13.2	1.9	Low	03:25	23	33
3	30.06.2022	49	27.6	3.6	Me-dium	10:35	24	72
4	20.07.2022	10	28.2	2.8	Me-dium	02:05	16	26
5	25.07.2022	20	22.8	2.1	Me-dium	05:45	18	38
6	28.07.2022	5	4.8	2.5	Me-dium	01:55	21	26
7	29.07.2022	9	4.8	1.8	Low	04:15	22	31
8	01.08.2022	7	16.8	1.9	Low	02:25	20	28
9	02.09.2022	8	34.8	1.9	Low	01:40	23	31
10	07.09.2022	29	30	4.1	High	05:45	24	53
11	14.09.2022	20	25.2	2.5	Me-dium	05:35	23	42
12	16.09.2022	51	10.2	2	Low	19:55	25	75
13	26.09.2022	18	12	1.6	Low	08:45	25	43
14	01.10.2022	34	7.2	2	Low	13:45	25	58
15	02.10.2022	25	11.4	2.2	Me-dium	09:25	25	50
16	08.10.2022	6	7.8	0.9	Low	07:25	24	30

Appendix B: Personal Declaration

I hereby declare that the submitted thesis is the result of my own, independent work. All external sources are explicitly acknowledged in the thesis.

Zurich, 16.01.2026 Damian Pfenninger